NATIONAL HURRICANE RESEARCH PROJECT

REPORT NO. 46

Some Aspects of Hurricane Daisy, 1958

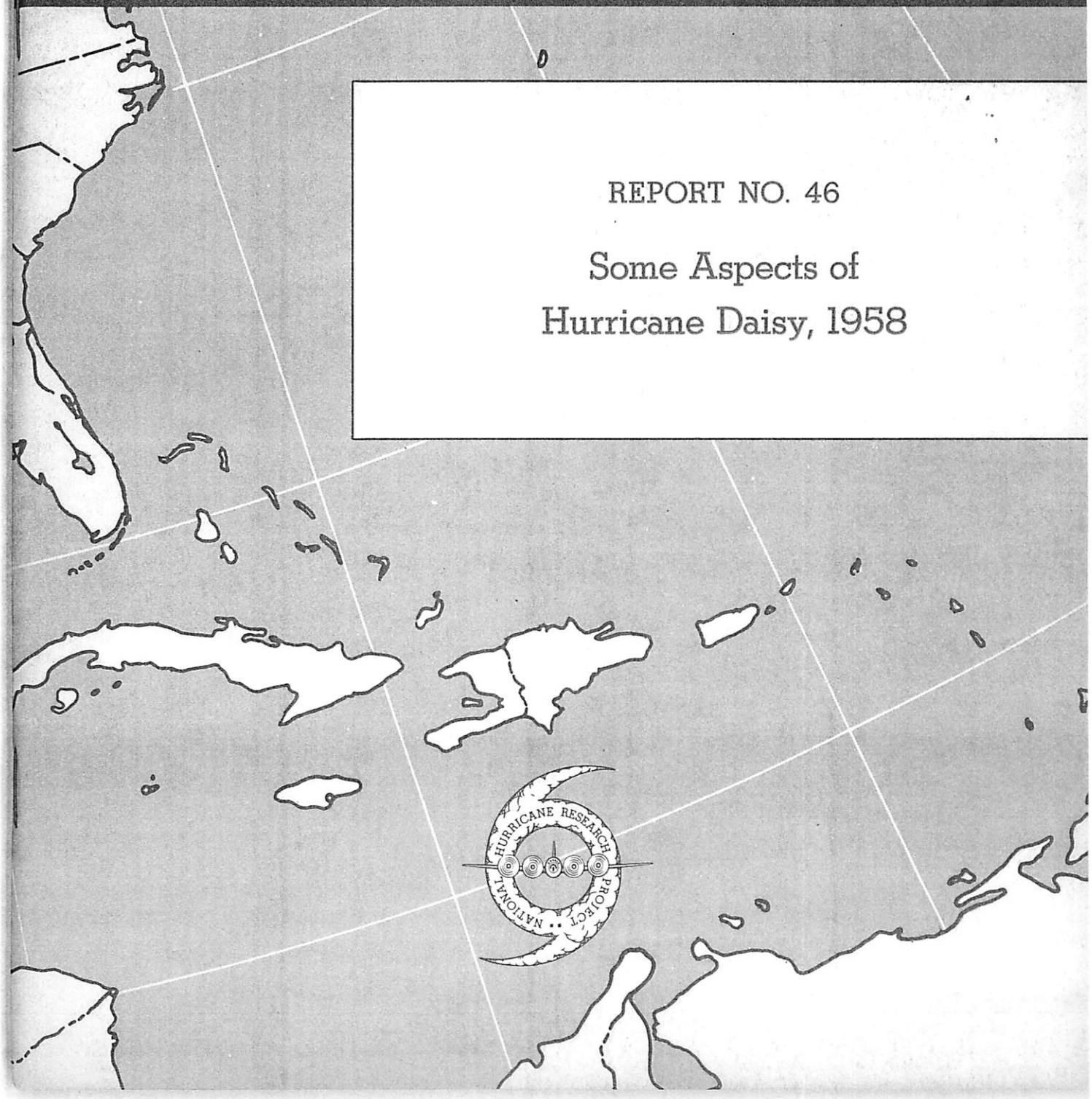

U. S. DEPARTMENT OF COMMERCE
Luther H. Hodges, Secretary
WEATHER BUREAU
F. W. Reichelderfer, Chief

NATIONAL HURRICANE RESEARCH PROJECT

REPORT NO. 46

Some Aspects of Hurricane Daisy, 1958

by
Herbert Riehl
Colorado State University
and
Joanne Malkus
Woods Hole Oceanographic Institution

Contrbution No. 1156 from the Woods Hole Oceanographic Institution

Washington, D. C.
July 1961

NATIONAL HURRICANE RESEARCH PROJECT REPORTS

Reports by Weather Bureau units, contractors, and cooperators working on the hurricane problem are pre-printed in this series to facilitate immediate distribution of the information among the workers and other interested units. As this limited reproduction and distribution in this form do not constitute formal scientific publication, reference to a paper in the series should identify it as a pre-printed report.

No. 1. Objectives and basic design of the NHRP. March 1956.
No. 2. Numerical weather prediction of hurricane motion. July 1956.
Supplement: Error analysis of prognostic 500-mb. maps made for numerical weather prediction of hurricane motion. March 1957.
No. 3. Rainfall associated with hurricanes. July 1956.
No. 4. Some problems involved in the study of storm surges. December 1956.
No. 5. Survey of meteorological factors pertinent to reduction of loss of life and property in hurricane situations. March 1957.
No. 6. A mean atmosphere for the West Indies area. May 1957.
No. 7. An index of tide gages and tide gage records for the Atlantic and Gulf coasts of the United States. May 1957.
No. 8. Part I. Hurricanes and the sea surface temperature field. Part II. The exchange of energy between the sea and the atmosphere in relation to hurricane behavior. June 1957.
No. 9. Seasonal variations in the frequency of North Atlantic tropical cyclones related to the general circulation. July 1957.
No. 10. Estimating central pressure of tropical cyclones from aircraft data. August 1957.
No. 11. Instrumentation of National Hurricane Research Project aircraft. August 1957.
No. 12. Studies of hurricane spiral bands as observed on radar. September 1957.
No. 13. Mean soundings for the hurricane eye. September 1957.
No. 14. On the maximum intensity of hurricanes. December 1957.
No. 15. The three-dimensional wind structure around a tropical cyclone. January 1958.
No. 16. Modification of hurricanes through cloud seeding. May 1958.
No. 17. Analysis of tropical storm Frieda 1957. A preliminary report. June 1958.
No. 18. The use of mean layer winds as a hurricane steering mechanism. June 1958.
No. 19. Further examination of the balance of angular momentum in the mature hurricane. July 1958.
No. 20. On the energetics of the mature hurricane and other rotating wind systems. July 1958.
No. 21. Formation of tropical storms related to anomalies of the long-period mean circulation. September 1958.
No. 22. On production of kinetic energy from condensation heating. October 1958.
No. 23. Hurricane Audrey storm tide. October 1958.
No. 24. Details of circulation in the high energy core of hurricane Carrie. November 1958.
No. 25. Distribution of surface friction in hurricanes. November 1958.
No. 26. A note on the origin of hurricane radar spiral bands and the echoes which form them. Feb. 1959.
No. 27. Proceedings of the Board of Review and Conference on Research Progress. March 1959.
No. 28. A model hurricane plan for a coastal community. March 1959.
No. 29. Exchange of heat, moisture, and momentum between hurricane Ella (1958) and its environment. April 1959.
No. 30. Mean soundings for the Gulf of Mexico area. April 1959.
No. 31. On the dynamics and energy transformations in steady-state hurricanes. August 1959.
No. 32. An interim hurricane storm surge forecasting guide. August 1959.
No. 33. Meteorological considerations pertinent to standard project hurricane, Atlantic and Gulf coasts of the United States. November 1959.
No. 34. Filling and intensity changes in hurricanes over land. November 1959.
No. 35. Wind and pressure fields in the stratosphere over the West Indies region in August 1958. December 1959.
No. 36. Climatological aspects of intensity of typhoons. February 1960.
No. 37. Unrest in the upper stratosphere over the Caribbean Sea during January 1960. April 1960.
No. 38. On quantitative precipitation forecasting. August 1960.
No. 39. Surface winds near the center of hurricanes (and other cyclones). September 1960.
No. 40. On initiation of tropical depressions and convection in a conditionally unstable atmosphere. October 1960.
No. 41. On the heat balance of the troposphere and water body of the Caribbean Sea. December 1960.
No. 42. Climatology of 24-hour North Atlantic tropical cyclone movements. January 1961.
No. 43. Prediction of movements and surface pressures of typhoon centers in the Far East by statistical methods. May 1961.
No. 44. Marked changes in the characteristics of the eye of intense typhoons between the deepening and filling states. May 1961.
No. 45. The occurrence of anomalous winds and their significance. June 1961.

CONTENTS

SOME ASPECTS OF HURRICANE DAISY, 1958

Herbert Riehl
Colorado State University

Joanne Malkus
Woods Hole Oceanographic Institution

[Manuscript received Apr. 17, 1961; revised May 22, 1961]

ABSTRACT

Observations from research flight missions into hurricane Daisy (1958) are utilized to compute the budgets of heat, moisture, kinetic energy, and momentum. Calculations are performed for a period when the cyclone was just becoming a hurricane, and for a second period, two days later when it had attained maturity.

The level of non-divergence separating lower inflow from upper outflow was quite high near 500 mb. Mass flow increased considerably between the two days, but rainfall remained quite moderate for a severe hurricane. The radiation heat sink was small compared to the oceanic source so that the system was "open" within the confines of the study. If all ascent took place in the hard radar echoes, the mean vertical speed there was about 7 meters per second. Without such localized ascent, heat balance could not have been achieved. Heat budget computations permitted assessing the fraction of mass flow reaching upper levels in undilute "hot" cumulonimbus towers and estimation of the number of such towers required, to compare with previous photographic studies. Hot towers proved to be the dominant mechanism of raising warm air to upper levels, particularly in the inner core. However, because of the high level of non-divergence the constraint known as ventilation was active. It is shown not to have been a severe deterrent upon Daisy, nor was it the reason this did not become an extreme storm.

Kinetic energy balance was obtained readily on the first day. Import of kinetic energy through the outermost radius was small, so that most of the energy dissipated in the interior was also produced there by the pressure forces. Ground and internal friction were about equal. The kinetic energy source shifted outward as the storm grew, so that on the day of maturity large inward transport took place. The internal source also increased but wind speeds failed to rise correspondingly. Hence ground friction was inadequate to balance production plus import, and large internal dissipation had to be invoked. This dissipation must be assigned largely to vertical eddies. If ascribed to horizontal eddies, the coefficient of lateral exchange becomes so large that momentum budget requirements cannot be fulfilled by a large amount.

It is concluded from the study that the important mechanisms of the hurricane core can be well represented in a two-dimensional framework, provided the essential effects of the buoyant cumulonimbus towers are properly introduced or parameterized therein. The two-dimensional flow of mass is shown in relation to the fields of heat, momentum, and vorticity. The law of conservation of potential vorticity appears to be well satisfied along the stream tubes of the mean motion.

1. INTRODUCTION

In a previous study Palmén and Riehl [22] calculated the budgets of angular momentum kinetic energy, and heat for a hurricane possessing a mean structure as determined by Hughes [11] and E. Jordan [13] from Pacific Ocean data. Because of the sparse and uneven distribution of observations, which were usually almost entirely lacking in the innermost 100 nautical miles, analyses had to be confined to the peripheral regions of a composited "mean hurricane." It has been of much interest to repeat this experiment in the core of an individual hurricane in various stages of development. The aircraft program of the National Hurricane Research Project of the U. S. Weather Bureau (hereinafter referred to as NHRP) was designed with this as a major part of its purpose. Here, we carry out, from their data, a budget study of the core of hurricane Daisy, 1958, with several definite objectives in mind.

Preliminary results from the NHRP program pointed to the vital importance of the core region, and, in particular, to highly concentrated convective processes within it, in the development and maintenance of the hurricane engine. It is commonly within the inmost 50-100 n.mi. that the extreme pressure gradients are generated which are responsible for the furious winds. In a semi-theoretical model, the writers (Malkus and Riehl, [19]) showed that establishment of these pressure gradients requires both an enhanced oceanic heat source and, concomitantly, a means to raise surface air of increased heat content to great heights; the latter condition apparently is the difficult one to meet. To achieve this, a selective buoyancy or "hot tower" mechanism was suggested (Malkus [17]), which has received support from cumulonimbus dynamics and photographic cloud measurements in hurricane Daisy (Malkus [18], Malkus, Ronne, and Chaffee [20]). We postulated that all, or nearly all, the mass reaching great heights in the core ascends rapidly in a few nearly undilute convective "hot" towers, rather than by a uniform and gradual "mass circulation." Now we wish to inquire whether these processes are consistent with and deducible from the azimuth-averaged thermal motion, and energy structure of the actual storm core, and to test the predicted relationships of the model in the framework of the overall storm budgets computed from the NHRP wind, temperature, and moisture data. What are the roles of the various scales of motion in establishing the budgets of the core? If the important processes are in fact concentrated into restricted convective regions, how much usefulness or meaning does an azimuth-averaged picture possess? Can it serve as a basis for developing numerical or theoretical models of predictive ability?

The rarity of the hurricane phenomenon and its development only under specialized synoptic conditions also suggest critical relationships to be sought between the core of an incipient storm, its periphery, and the surrounding large-scale circulations, both normally as brakes and exceptionally as brake releasers or vortex initiators. "Ventilation" by cooler, drier outside air has been postulated (Simpson and Riehl [30]) as a brake; tropical disturbances which fail to become hurricanes are frequently found to suffer cross-flow of mid-tropospheric air of low heat content. Whether removal of critical brakes is adequate to start a hurricane, or whether one or more specific destabilizing mechanisms are also necessary has remained conspicuously unclarified, although forcing by external circulations appears indicated in a majority of cases. Some workers, for example, have advocated the possible

importance of lateral eddy momentum transports in the deepening process. A basic question is whether or not these, or other, asymmetrical interactions are vital and at what stages, or whether the key features may be modeled in simplified symmetrical coordinates through all or a major part of the storm's life cycle.

Fully adequate data to resolve these questions are not yet available. Nevertheless, in spite of many shortcomings, it is considered worthwhile to present computations from the NHRP's Daisy flights as a "lead off" in the quantitative description of a hurricane's internal mechanisms. Several successive days of multi-level records on a single storm, from incipience to maturity, is a monumental and not readily reproducible observational undertaking. Our aim is to make the most of this achievement by treating those aspects of the questions to which the data are best suited; we can thereby assess the magnitudes of some of the interacting processes and scales of motion at more than one stage in a single hurricane's life cycle, with the hope of determining which are most vital and which may be parameterized or possibly ignored. Although it must be stated clearly at the outset that these results are tentative, and subject to revisions by future measurements, their very inadequacies may lead to more fruitful and penetrating questions to be pursued with improved observational facilities as these become available.

Hurricane Daisy began to develop in the Bahamas on August 23-24, 1958, and had not quite attained hurricane intensity when it was first penetrated by NHRP aircraft on August 25. During this and subsequent days numerous research flights were conducted; Daisy's track is shown in figure 1. Here we shall treat August 25 when the hurricane was immature and growing, and August 27 when the winds reached their peak of about 115 knots in the middle troposphere, when the surface pressure was below 950 mb., and when steady state in the moving system was attained as nearly as can be expected in actuality.

The research aircraft of NHRP and their instrumentation have been described elsewhere[10]. Prescribed flight patterns, in a form resembling boxes about the storm center or leaves of a clover radiating therefrom, were executed. The data are presented by NHRP as a function of coordinates relative to the moving storm center, from its radar location, as well as in latitude and longitude. Analyses of the Daisy wind, temperature, and humidity data have been prepared by Colón et al. [2]. Cloud maps were constructed from the aircraft nose camera films by Malkus et al. [20], who have discussed the sampling problem posed by the relation between the flight paths and the cloud patterns. Studies of the airborne radar in Daisy were made by those authors and also by Jordan et al. [12]. In this article we shall be concerned mainly with the three-dimensional distribution of wind, temperature, moisture, and height of isobaric surfaces. At each flight level, averages were constructed of each property to determine its mean distribution with radial distance and azimuthal departures from this mean. On August 25 extensive tracks were flown at 830, 560, and 237 mb., with additional legs at 960 and 915 mb., so that distributions throughout the troposphere were readily constructed for the inner 100 n. mi. On August 27, the flight altitudes were 620 and 247 mb., so that more extrapolation was required. Surface ship observations, composited with respect to the center over 12-hour intervals, supplemented the aircrart data; however, on August 27 no ships were situated inside the 100-mi. radius.

2. THE MASS BUDGET

In an analysis of hurricanes it is logical to determine the flux of any property through cylindrical walls concentric about the core. We shall adopt a quasi-cylindrical coordinate system θ, r, p, centered on Daisy, with velocity components u, v, w, respectively. The radius r is taken positive outward and θ, the azimuth angle, positive counterclockwise. Flux of any property through the vertical walls of the cylinder may be brought about by the mass circulation flowing in at low levels and out at high levels, and by asymmetries of property around the cylinder acted on by the radial wind components. As a first step in flux calculations, mass balance must be computed.

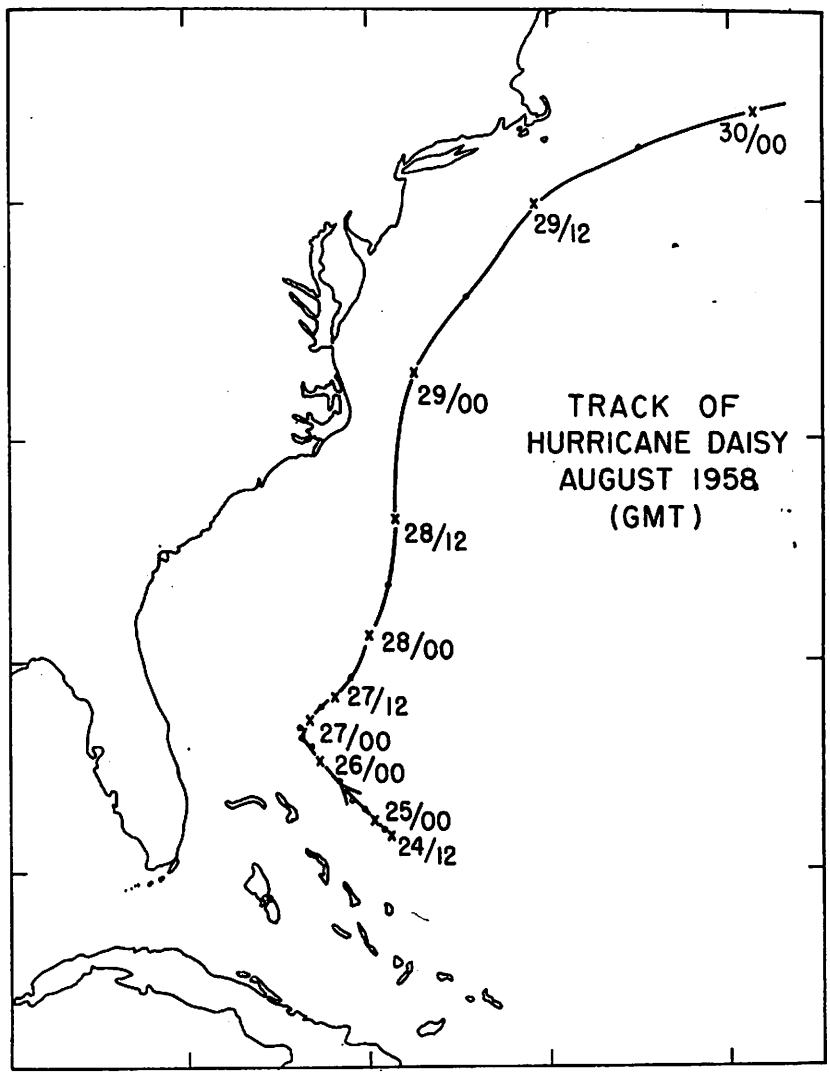

Figure 1. - Track of hurricane Daisy, August 24-28, 1959.

For this purpose it should be noted that even in strongly deepening cyclones the change of mass inside a given cylinder is so small that it is fully within range of error of the wind measurements and must be neglected. Hence mass balance must be obtained by setting

$$\int_{p_0}^{p_H} v\,dp = 0 \qquad (1)$$

where p_0 is the surface pressure and $p_H = 0$, alternatively the pressure at the top of the storm, if such a place can be found. In practice p_H does exist and may be defined as the lowest pressure to which buoyant clouds will mainly penetrate from the surface layer. From cloud observations (Malkus et al.[20]) and buoyancy calculations $p_H \sim 150$ mb. (about 47,000 ft.) on August 25 and $p_H \sim 100$ mb. (about 54,000 ft.) on August 27. Above p_H the circulation

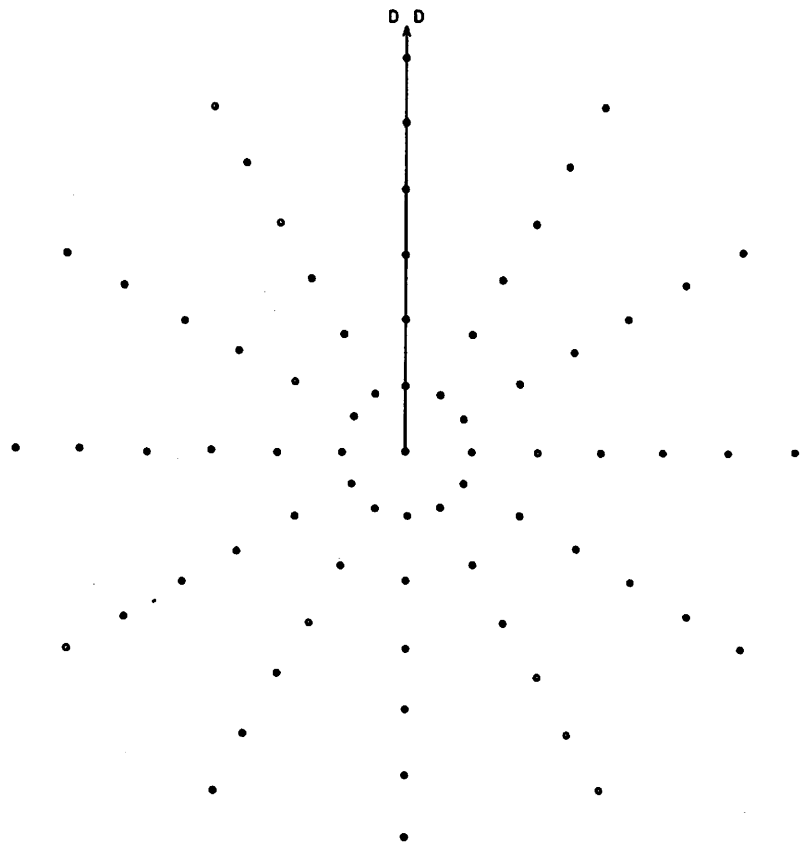

Figure 2. - Grid sample for hurricane calculations; azimuth 30° interval; radial interval arbitrary, usually taken as 10 n.mi.

should be quasi-steady. That this is likely to be the case has been shown by many radio-wind ascents in tropical storms in several oceans. The stratospheric easterlies remain undisturbed as far as one can tell (Riehl [25]). Groening [9] has demonstrated this steady stratospheric flow field for August 25 in the periphery of Daisy. No radio-wind data, of course, existed in the central region. There p_H must be assumed, but the cloud observations strongly support the validity of the assumption.

The procedure for determining mass balance is as follows:

1. The v-field is analyzed at all available flight levels.

2. The analysis is tabulated on a polar grid (fig.2).

3. $\bar{v}$ is computed at each radius, where the bar denotes averaging with respect to the azimuth angle.

4. $\bar{v}$ is plotted against pressure on each radius and a profile is drawn. From this profile values of $\bar{v}$ are determined for layers of 50-mb. or 100-mb. thickness and summed from p_0 to p_H.

According to equation (1) the sum must vanish.

Given enough flight levels and reliable data, there should be no problem in satisfying equation (1). In actuality, analysis of the v-fields turned out to be a difficult task so that the $\bar{v}$-values are not stable. Contrary to early expectations the v-fields have not always shown consistent patterns along individual flight legs, triangles or boxes. Further, an aircraft recrossing a point where it had been earlier, often yielded a v-value different from the first one, at times even with opposite sign. Several possible reasons may be cited for these difficulties:

(a) Errors in wind measuring equipment or evaluation. Since the v-component is the weak flow component it is sensitive to such errors.

(b) Errors in center fixing. Unfortunately a hurricane seldom yields a precise point which may be taken as the center, but there is a flat area to which a center must be assigned. This affects v, especially at small radii.

(c) Errors in estimating storm propagation. In order to obtain a "synoptic" picture, the information gathered on successive flight legs must be "composited" with respect to the moving center. Hence its propagation rate must be known. While the mean 24-hour motion can be estimated quite accurately, this does not always hold for small time intervals such as 1 or 2 hours.

(d) Traveling micropatterns within the general envelope. Motions with the scale of the convective bands are quite active, and this motion may be unsteady in time and space. Compositing of flight legs which are successive in time, cannot readily take account of such transient small-scale features.

(e) Time changes of the whole vortex. On August 25, for instance, Daisy was deepening while the aircraft remained in the storm for 8 hours or more.

In view of these data problems it was necessary at times to make considerable compromises in analyzing the v-field; at other times a good fit could be obtained quite readily.

Surface inflow: For the purpose of determining the surface mass flow, ship reports were composited for 12-hour periods with respect to the moving center, i.e., three 6-hour charts plus intermediate data were combined. These reports, also far from homogeneous, were first averaged over areas with radial length of 60 n. mi. (1° latitude) and arc length of 30°. Inside the 1° radius an attempt was made to average over shorter radial lengths, where data were sufficient to permit this. On August 25 flight data at 960 mb. were used for this purpose. Then an analysis was performed with smoothing and $\bar{v}$ was computed for different radii. Next the quantity $\bar{v} \times r$, which is proportional to mass flow, was plotted on graph paper and smooth curves were drawn.

Figure 3 portrays the rise of surface mass inflow from the early stages of Daisy up to the time of maturity. An orderly increase took place day by day as the storm deepened. Central pressure and maximum inflow thus were inversely correlated; the regression found by Krueger [15] on six previous Atlantic hurricanes held well. The size of the storm increased with its intensity. On August 24 and 25 the limit of mass flow was situated near the 5° radius, and average convergence was confined to a belt about 100 n.mi. wide around the center. On the last two days tremendous expansion took place. The hurricane boundary could no longer be ascertained; maximum inflow occurred 200-300 n. mi. from the center just as in the hurricanes treated by Krueger. Hence the mass flow was convergent over the entire inner area (cf. also Malkus and Riehl [19]). On August 26, ships were still traveling near the cyclone center, but on the 27th the innermost point to be obtained was at the 2° radius. From there the mass flow profile had to be extrapolated inward. While the precise course of this curve is uncertain, its general character probably is reliable.

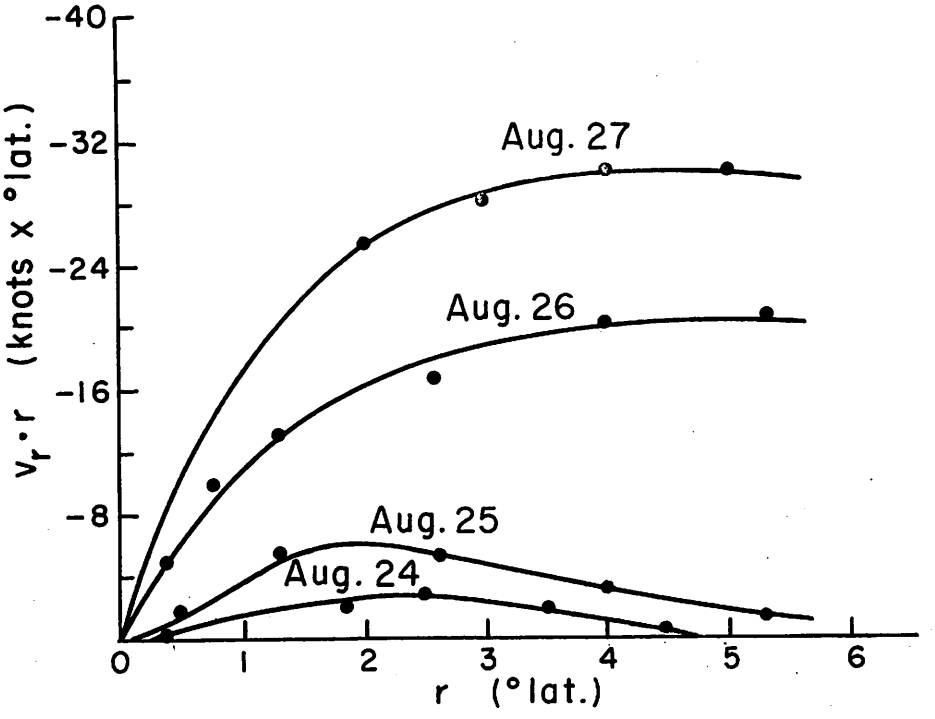

Figure 3. - Growth of mass circulation in Daisy. Values at surface, constructed from ship reports. The hurricane eye, which was very small, is neglected on the distance scale shown.

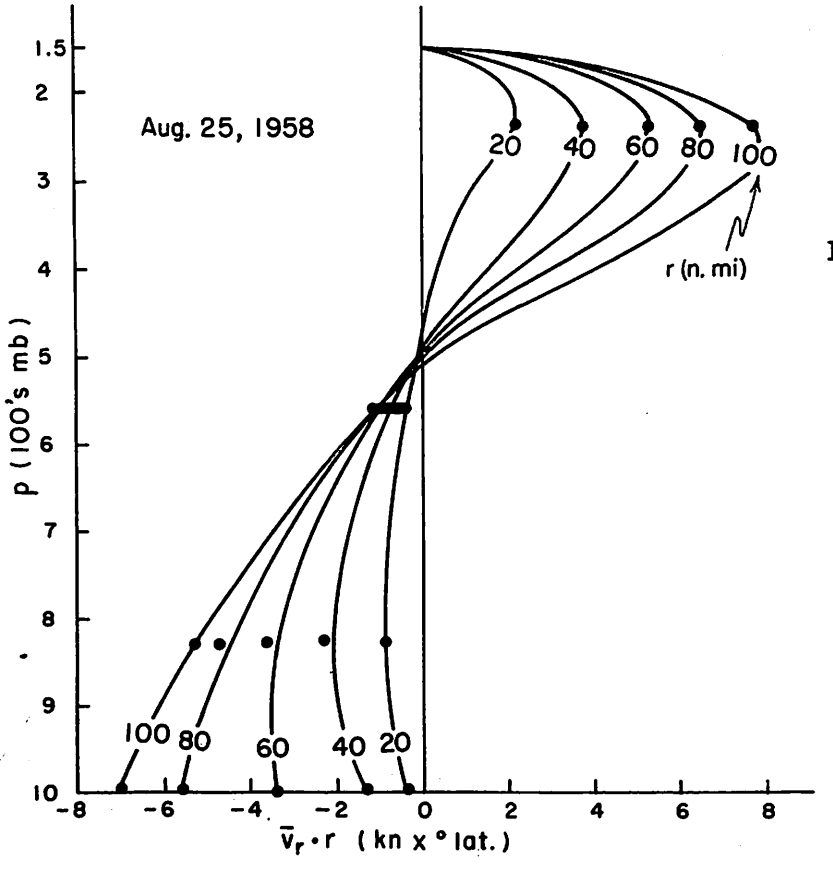

Figure 4. - Profiles of mass flux against pressure for different radii, August 25.

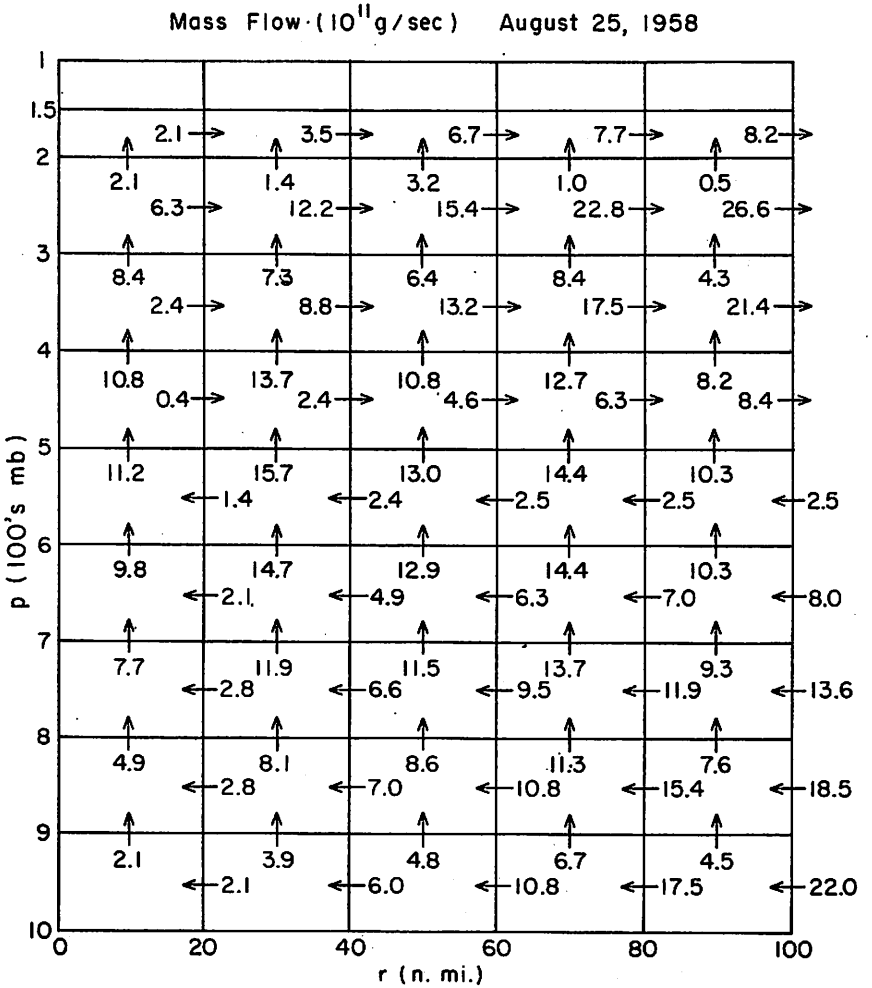

Figure 5. - Mass flow on August 25.

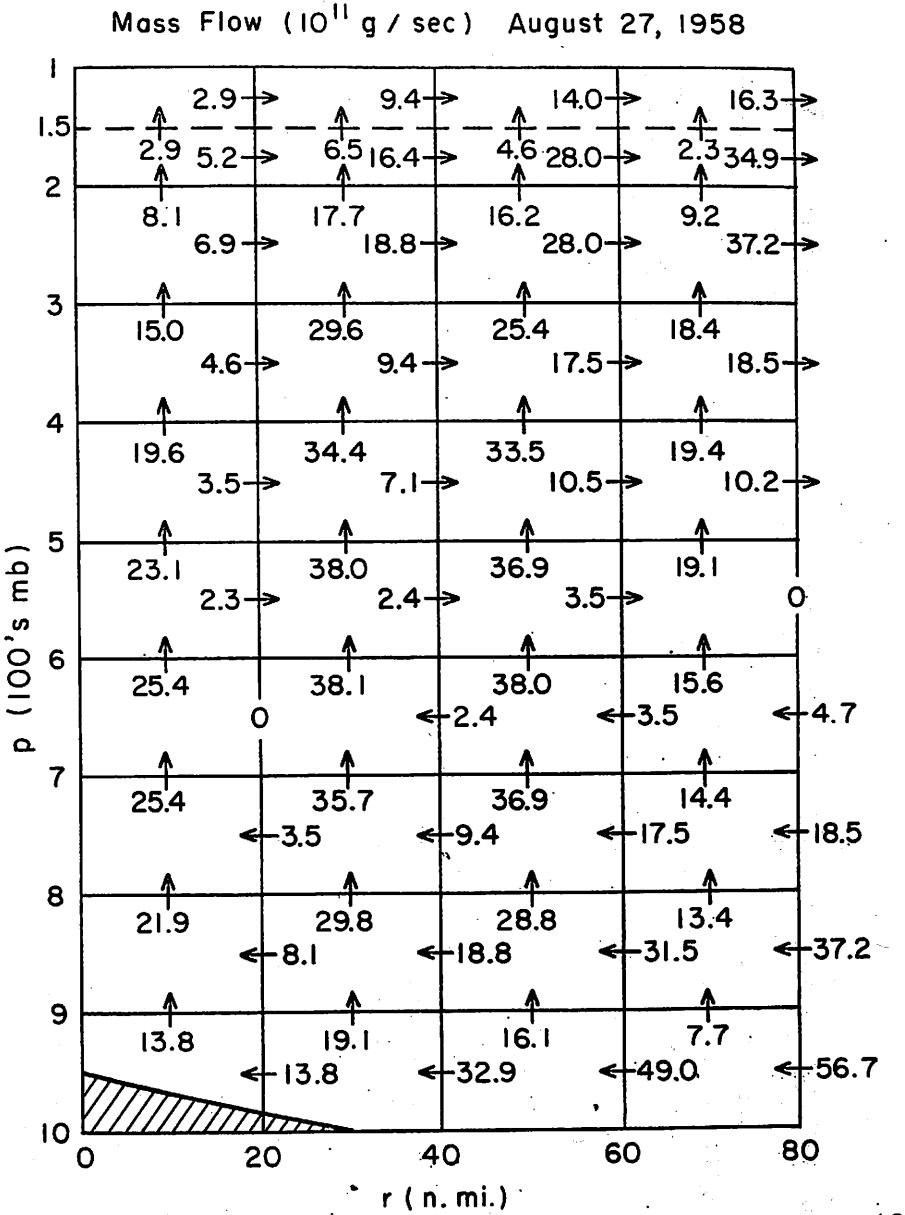

Figure 6. - Mass flow on August 27. ⟶

Mass transport diagrams: The $\bar{v}$-value for the surface and the flight levels were entered on diagrams of $\bar{v}$ x r against pressure on a linear scale, and curves were drawn as illustrated in figure 4 for August 25. Then $\bar{v}$ x r was tabulated over layers of 100-mb. thickness up to 200 mb. and in 50-mb. steps higher up at each radius; mass at pressures greater than 1000 mb. was neglected. As pointed out, the sum of these values should vanish after proper weighting. This condition was closely met by the curves at the 20 and 40 n. mi. radii in figure 4. At the three outer radii inflow exceeded outflow, and some downward revision of the inflow was made. It is probable that the 830-mb. level gave too much indraft. At 560 mb., all values were so close together that a band rather than a series of five points has been entered in figure 4. Analysis at this level was particularly difficult but the net result, as also on other occasions, was that light inflow prevailed. Thus the level of non-divergence was located near 500 mb., a higher altitude than previously expected.

From curves as illustrated in figure 4 mass flow diagrams were constructed (figs. 5-6). A few irregularities remain, but in general vertical and lateral consistency is good. On August 27 the inflow extended upward to about 500 mb. as on August 25, but the percentage of the inflow taking place in the surface layer increased from one-third to one-half. Thus, while the middle troposphere is revealed as a constraint upon the hurricane by means of the "ventilating" mechanism, the basic statement still stands that the principal inflow must occur in the surface layer in order for a hurricane to occur (see end of Section 6).

Figures 5 and 6 are not meant to imply uniform radial and vertical mass flow in each of the rings. It has long been known that the radial velocity component at the surface is not symmetrical at any radius. In a statistical treatment of North Atlantic hurricanes of 1954-55 Ausman [1] demonstrated that a large sector with outflow usually exists, even in quasi-stationary cases. Most flight data contain similar asymmetries. Further, from radar observations and cloud photography, the mass ascends in rather narrow bands covering only a small fraction of a hurricane's area. Malkus et al. [20] pointed out that the area covered by "hard" radar echoes on August 25 was 6 percent as far out as the 55 n. mi. radius. If all ascent at the level of non-divergence (500 mb.) took place in an area of the size of the hard echoes, the average vertical velocity in the bands was 7.2 m. $sec.^{-1}$ inside the 20-mi. radius, 3.2 $m.sec.^{-1}$ from 20 to 40 mi., and 1.6 $m.sec.^{-1}$ from 40 to 60 mi., a quasi-logarithmic decrease illustrated in figure 7.

3. THE TOTAL HEAT BUDGET AND AIR-SEA EXCHANGE

Introductory comments: The heat export from any cylindrical volume is closely given by

$$\mathrm{div}(H) \equiv \int\int (gz + c_p T + Lq) c_n \, d\sigma \, \frac{dp}{g} .$$

Here div(H) is the integral of energy flux divergence, g the acceleration of gravity, z height, c_p specific heat at constant pressure, L latent heat of

condensation, q specific humidity, T temperature, c_n the wind component normal to the boundary and σ the surface of the cylinder. On the right side the first term denotes potential energy (in heat units), the second enthalpy, and the third latent heat energy. We shall define

$$Q \equiv gz + c_p T + Lq.$$

For a total energy budget kinetic energy should also be included. Its contribution to the heat budget, however, is very small compared to that of the other energy forms, and it will be considered separately later on. Since we are interested in fluxes with respect to the moving center, we shall let the cylinder travel with the storm and denote variables measured in the moving coordinate system with the subscript R. With this definition, continuity demands that

$$\frac{\partial Q^*}{\partial t_R} = -\mathrm{div}_R(H) + Q_{eR} + Q_{sR} - R_{aR}. \quad (2)$$

Here the star denotes values integrated over the mass inside the cylinder, and the heat source $S = Q_{eR} + Q_{sR} - R_{aR}$, where Q_{eR} and Q_{sR} are latent and sensible heat transfer from sea to air, and R_{aR} is the net tropospheric radiational heat loss. The subscript R will hereafter be omitted from the source and sink terms.

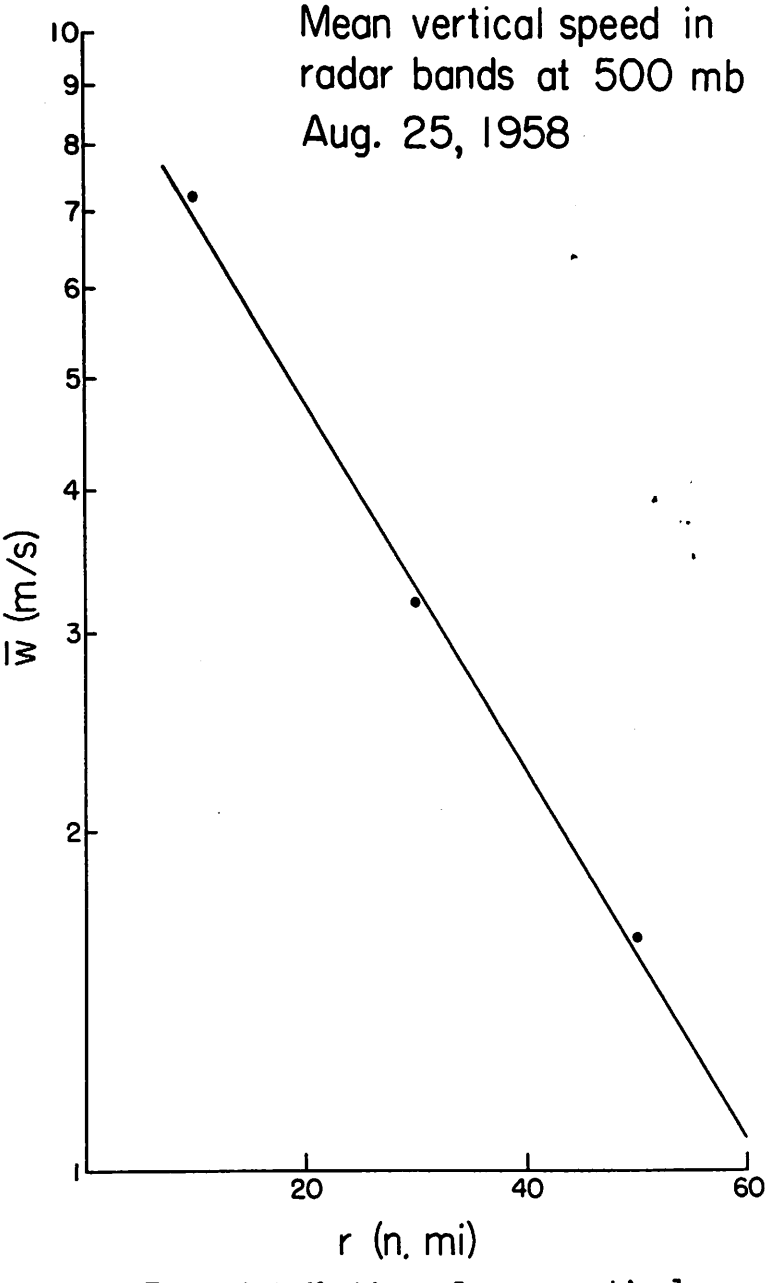

Figure 7. - Distribution of mean vertical velocity with radius, assuming that all ascent takes place in an area comparable to that of the radar bands. Note this special definition of the bar over the w.

The change in total heat content (equation (2)) is brought about by changes in latent heat content and in $(gz + c_p T)$. Thus:

$$\frac{\partial}{\partial t_R}(gz + c_p T)^* = -\mathrm{div}_R(h) + Q_s + LP - R_a, \quad (3)$$

$$L \frac{\partial q^*}{\partial t_R} = -\text{div}_R (Lq) + Q_e - LP. \qquad (4)$$

Here P is precipitation, and $\text{div}_R(h) + \text{div}_R(Lq) = \text{div}_R(H)$. Equation (4) permits later calculation of a separate moisture budget, including precipitation.

Observations of heat and moisture: For the purpose of determining the fluxes, data on temperature and height of the isobaric surface (altimeter correction D) were available at all flight levels; in addition, dewpoint temperatures (T_d) were measured on several of the lower-altitude flights. Temperatures and dewpoints at ship's deck level, also sea surface temperatures, were composited on August 25 and, as far as possible, on August 27 from the file of ship reports already mentioned and from 960-mb. flight data on August 25. Analyses of T, D, and T_d were performed on each flight level and tabulated on the grid of figure 2. Then T_d was converted to specific humidity q, and $\overline{T}$, $\overline{D}$, and $\overline{q}$ were computed at 10-mi. radial intervals on each flight level. The bar denotes the azimuthal average. Next $\overline{T}$ was plotted on tephigrams at radii of 10, 20, 40, 60, and 80 n.mi.; curves of best fit were drawn to represent mean vertical soundings. These curves were extended beyond the B-47 flight level until they intersected the radiosonde ascents of the northern Bahamas. The specific humidities were treated similarly as far as possible; when these data were not recorded, the relative humidity was assumed to be 90 percent.

Several results were slightly awkward, especially in the middle troposphere , where temperatures frequently were 1°-3°C. cooler than expected, and the specific humidity at times exceeded saturation values. Possible causes of the low temperatures - especially whether real or instrumental - have been debated since the inception of these measurements. No satisfactory explanation is at hand, and it remains for new observational programs to apply conclusive tests. For this paper the uncertainty is not of decisive importance. In order to avoid excessive vertical instability below, and stability above, the flight levels between 500 and 600 mb., $\overline{T}$ was raised 1° - 2°C. on several occasions. The supersaturated dewpoints were disregarded as most likely due to observational shortcomings. If this procedure was unwarranted, some revision of the heat flux calculations will become necessary. This would not affect the general nature of most results, particularly on August 25 when these difficulties arose only rarely.

Figure 8 illustrates a sounding in which hardly any adjustment of temperature was needed. Ship data in the surroundings of Daisy gave 26° - 27°C. at pressures of about 1010 mb. At the 20-mi. radius, surface pressure was estimated as close to 1005 mb. These data, plus the adiabatic assumption, established the lowest point of the hurricane sounding of figure 8. From there a dry-adiabatic lapse rate can be drawn to the measured point at 960 mb. which agrees with the general observation of dry-adiabatic conditions in the subcloud layer. The 960 mb. flight leg was chosen because the cloud base was situated near this pressure in the interior of the storm; the airplane flew just underneath the clouds. With the top of the subcloud layer near 960 mb., a change in lapse rate should be expected very close to this level. This is borne out by the points at 915 mb. and 830 mb. Omitting three excessive dewpoints, the whole temperature curve is readily established. Above 500 mb.

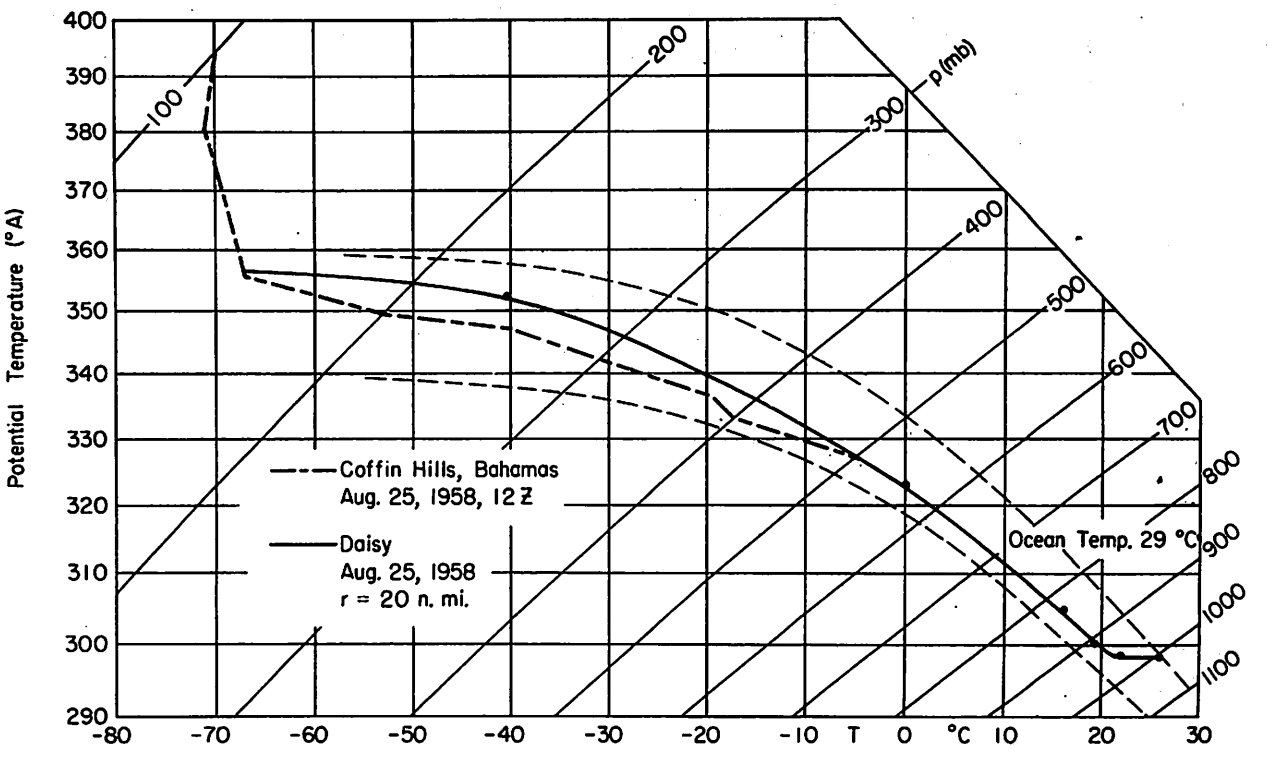

Figure 8. - Tephigram showing composited sounding for Daisy on August 25 at the 20-mi. radius and the upper portion of the ascent at the nearest radiosonde station. Light dashed curves are moist adiabats. Ocean surface temperature, T_o, from ship reports was 28°-29°C.

the sounding was 2°-3°C. warmer than the nearest ascent in the Bahamas. The top of the warm layer was situated near 150 mb. which agrees well with the measured height of cloud tops (Malkus et al. [20]). Below 500 mb. the lapse rate was slightly greater, and above 500 mb. it was slightly more stable than moist-adiabatic. Such a structure is reasonable. In the low and middle troposphere ventilation - to be discussed later - prevents the lapse rate from becoming fully moist-adiabatic. In the upper troposphere release of latent heat of fusion plus outward spreading of air which has ascended in the inner core (with equivalent potential temperatures up to 360°A) produce the small stability with respect to the moist-adiabatic ascent.

As a further test, the sounding of figure 8 may be checked for hydrostatic consistency against a vertical D-profile obtained independently from the aircraft's absolute altimeter. For this calculation the height of the 250-mb. surface was taken equal to the height of this surface as determined by radiosonde in the Bahamas. Agreement between D-values as calculated and as observed by the aircraft was well within the range of measurement errors.

For the lateral flux calculations it is most convenient to utilize values integrated over the same pressure intervals chosen for figures 5 and 6. For vertical fluxes, means over areas between two radii are needed; these will be denoted with a wavy ($\sim$) bar. Tables in the Appendix contain all necessary quantities for lateral flux calculations on August 25 and 27. Since on the

latter day only two missions were flown, the entire lower troposphere had to be interpolated. Hence the margin of uncertainty for all computations is greatest on this day.

Local changes of heat and moisture: The magnitude of $L\,\partial q^*/\partial t_R$ in equation (4) can be estimated from the moisture data in table A2 (Appendix). On August 25 the precipitable water content between the center and the 80-mi. radius, area-weighted, was 5.6 gm. cm.$^{-2}$; by the 27th it had risen to 6.5 gm. cm.$^{-2}$. This corresponds to a heat increment of 2.1 x 10^{12} cal.sec.$^{-1}$ which proves to be about one-third the source term and an order of magnitude smaller, relative to net advection. From table A4 the change in $c_p T + gz$ content between August 25 and 27 comes out 0.85 x 10^{12} cal.sec.$^{-1}$, or even smaller than the moisture change. On August 27 the cyclone attained maximum development, so that local change with respect to the center presumably was nil.

Lateral eddy transports of moisture and heat: The lateral component of flux divergence of a property N is determined from the radial transports

$$\iint \overline{Nv}_R \, r d\theta \, \frac{dp}{g} = \iint \overline{N}\overline{v}_R \, r d\theta \, \frac{dp}{g} + \iint \overline{N'v'}_R \, r d\theta \, \frac{dp}{g} \qquad (5)$$

where the first term on the right gives the transport by the mass circulation and the second that due to asymmetries around each cylinder. Asymmetries with respect to θ are denoted by primes and the subscript R has been omitted in the first term because $v \equiv v_R$. For evaluation of the eddy contribution only three flight levels were available: 830 and 560 mb. on August 25 and 620 mb. on August 27. The uncertainty concerning data is such that a fully reliable determination cannot be made. Values of the eddy transport of moisture and heat, as obtained on the 80-mi. radius are listed in Table 1. It may be noted that a moisture transport of 1 kt. x g.kg.$^{-1}$ over a layer of 500-mb. thickness gives 1.4 x 10^{12} cal. sec.$^{-1}$ and that a heat transport of 1 kt.x°C. corresponds to 0.6 x 10^{12} cal. sec.$^{-1}$ at the 80-mi. radius. Eddy fluxes of this order have the same magnitude as the local changes and are much smaller than the flux due to the mean motion.

Total heat balance: In evaluating equation (3) then, $\partial Q^*/\partial t_R$ may be set equal to zero. Then the total heat source $S = Q_e + Q_s - R_a$ is given by the net transport of heat through a cylinder. Figures 9 and 10 contain the lateral flux data and also the net heat source over areas with radial distance of 20 n.mi. as determined from $\mathrm{div}_R(H)$. The quantity $Q_a = Q_s + Q_e$ is obtained by setting

$$Q_a = \mathrm{div}_R(H) + R_a.$$

In a hurricane the main radiational surface presumably is transferred to the top of the outflow overcast which, as shown by cloud photographs, is very thick and may be assumed to act as a black body radiator in the first approximation.

Table 1. - Eddy moisture and heat fluxes

	Aug. 25 830 mb.	Aug. 25 570 mb.	Aug. 27 620 mb.
$\overline{v'_R q'}$ (kt. x g.kg.$^{-1}$)	-0.7	-1.5	0.7
$\overline{v'_R T'}$ (kt. x °C.)	-0.1	-1.2	-2.3

On August 25 the B-47 was quite close to the top of the thick cirrostratus at temperatures near -40° C., so that the cooling was about 0.24 ly. min.$^{-1}$ or 2.7×10^{12} cal.sec.$^{-1}$ inside the 80-mi. radius if all incident sunlight was reflected. This corresponds to a mean tropospheric cooling of 1°C. per day which appears reasonable and was adopted for estimating Q_a. It may be noted that there is a good chance that the net radiating surface was situated at a lower temperature on August 27. If so, the radiation cooling would have been even smaller on that day. At an effective radiation temperature of -60°C., for instance the cooling is 0.17 ly. min.$^{-1}$ Thus the hurricane outflow overcast, when thrust upward to high levels, protects the warm core.

From figures 9 and 10, Q_a was nearly twice as large as S on August 25, whereas the difference was small on August 27 and would be smaller with the assumption of a still higher and colder radiating shield. It should be noted that the value of S is uncertain to the extent that there are eddy transports of Q. As shown before, the eddy flux may be neglected in separate moisture and heat budgets. But the net energy export by the mass circulation is a small difference between the import of latent heat and the export of $gz + c_p T$. It is possible to visualize an eddy flux of the same magnitude. Due to data uncertainties and insufficient number of flight levels, this subject cannot be pursued further. The reasonable results in our next section on sea-air exchange suggest that this unknown eddy heat flux is not large.

The oceanic source and air-sea exchange: We should now like to be able to divide the total oceanic source into its latent and sensible heat contributions in order to complete an independent moisture budget. We should also like to examine the oceanic exchange requirements to compare with the model of Malkus ane Riehl[19] and to assess a drag coefficient for later use in constructing Daisy's momentum and energy budgets. All these objectives may be achieved if the exchange coefficients for the flux of heat, moisture, and momentum from ocean to air are identical. According to Priestley[23] this will hold at very small Richarson and "Richardson "flux numbers. The letter may be defined as

$$Ri_f = - \frac{gQ_s}{c_p T \ \tau_0 \ \partial u/\partial z} .$$

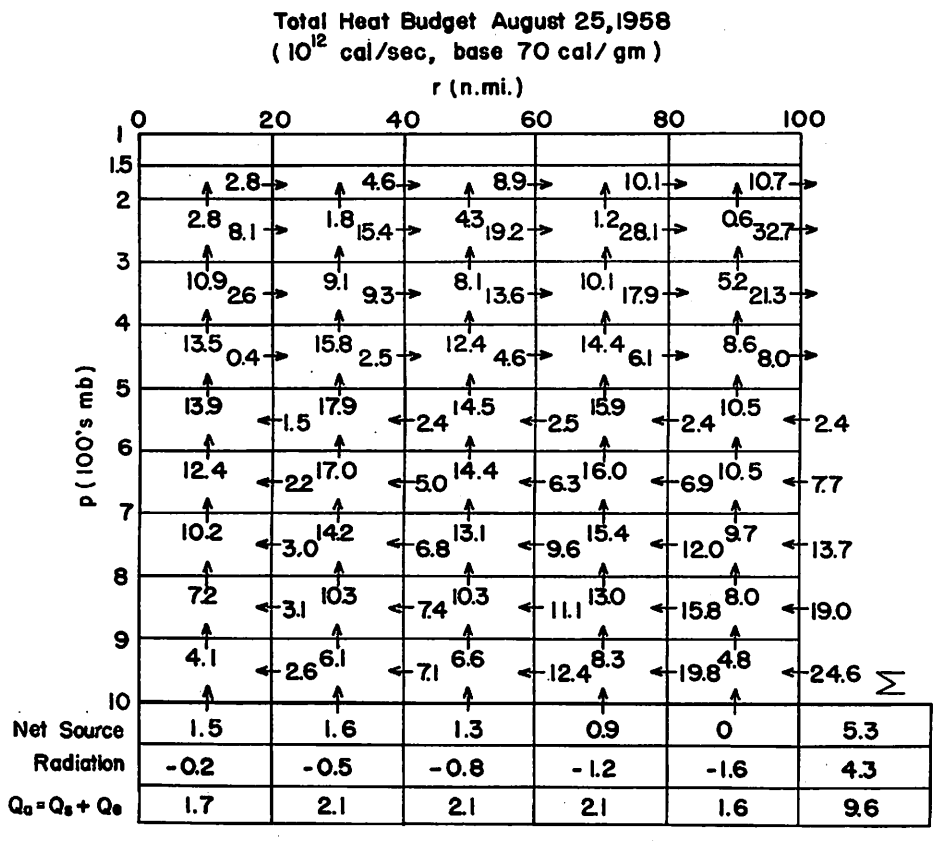

Figure 9. - Transport, sources, and sinks of total heat energy Q for Daisy on August 25. Lateral flows found by multiplication of lateral mass flow by $\bar{Q}$ - 70 (Table A8, Appendix). Vertical fluxes to meet continuity and net sources in radial intervals as residual. Total oceanic source Q_a, after allowance for radiation loss, in units 10^{12} cal.sec.$^{-1}$ in each radial interval.

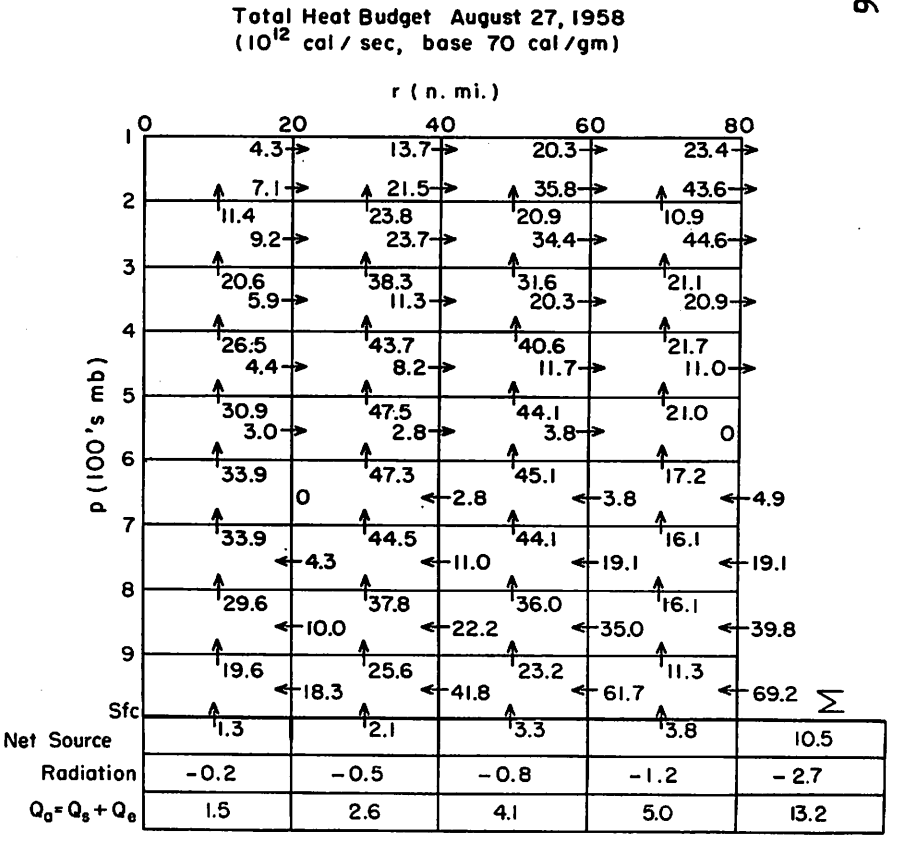

Figure 10. - Transports, sources, and sinks of total heat energy Q for Daisy on August 27. Procedure and notation same as figure 9.

By use of $Q_s = 0.5 \times 10^{-2}$ cal.sec.$^{-1}$, $\tau_0 = 10$ dyne cm.$^{-2}$, $\partial u/\partial z = 20$ m.p.s. 10 m.$^{-1}$, $Ri_f \sim 3.5 \times 10^{-3}$. Retrospectively, our exchange calculations show Ri_f never exceeds twice this value in Daisy. The Richardson number $Ri \approx - 10^{-3}$ for an air-sea temperature difference of 2°C. and wind shear as above. It appears that the criterion is well met. With this, Q_s/Q_e can be determined from the Bowen ratio

$$r_B = \frac{c_p}{L} \frac{T_0 - T_a}{q_0 - q_a}$$

where the subscripts "0" and "a" refer to the sea surface and ship's deck level, respectively. On the 25th, the ship reports gave $T_0 = 28° - 29°$ C. so we have taken $T_0 = 28.5$°C. and $T_0 - T_a = 2.5$°C. On August 27, ship reports were lacking; we have taken $T_0 = 28$°C. and $T_0 - T_a = 2$°C. since the storm center was about 150 n.mi. farther north. The drag coefficients, c_D, are computable alternatively from either of the well-known exchange formulas

$$\frac{Q_s}{A} = \rho \, c_p \, c_D \, u_a \, (T_0 - T_a)$$

$$\frac{Q_e}{A} = \rho \, L \, c_D \, u_a \, (q_0 - q_a)$$

where A is the ocean surface area, and u_a is the wind speed at ships' deck level. The specific humidity at the ocean surface, Q_0, was found (using tables) from the saturation q at the sea surface temperature, while the q_a's were taken from table A2, which gave values consistent with cloud base at about 970-960 mb. throughout. Table 2 shows the components and results of the exchange computation.

Except for the innermost radial interval on both days, the c_D's of table 2 are slightly smaller than careful experimental determinations (Deacon, Sheppard, and Webb [3]) would lead one to expect. According to these authors, drag coefficients of 2.2 - 2.5 x 10^{-3} were indicated for winds greater than 10 m.sec.$^{-1}$, with about 1.4 x 10^{-3} for normal trade-wind speeds of 6-7 m.sec.$^{-1}$ The smaller coefficients of table 2 may be due to omission of a small eddy Q export, or underestimation of the radiative sink, or other shortcomings of our data or procedures. Nevertheless, in view of the limitations, the results of the exchange computation are very satisfactory. The Bowen ratio averaged 0.18 on both the formation and mature days of Daisy, or 50-100 percent larger than found by Garstang [6] in moderate tropical disturbances. The oceanic latent heat source, relative to the normal trade, is up by a factor of 3-4 on the 25th and 5-6 on the 27th, while the sensible heat source has risen by factors

Table 2. - Air-sea exchange computation

A. August 25

$\rho = 1.2 \times 10^{-3}$ $T_0 = 28.5°C.$

	Radial Interval (n.mi.) 0-20	20-40	40-60	60-80	80-100
Q_a ($\times 10^{-12}$ cal.sec.$^{-1}$)	1.7	2.1	2.1	2.1	1.6
$T_0 - T_a$ (°C.)	2.5	2.5	2.5	2.5	2.5
$q_0 - q_a$ (g.kg.$^{-1}$)	5.3	5.5	5.5	5.6	5.8
r_B	0.19	0.18	0.18	0.18	0.17
A ($\times 10^{-14}$ cm.^{2})	0.43	1.29	2.15	3.01	3.87
Q_e/A (cal.cm.$^{-2}$sec.$^{-1}$)	3.32×10^{-2}	1.38×10^{-2}	0.83×10^{-2}	0.59×10^{-2}	0.36×10^{-2}
Q_s/A (cal.cm.$^{-2}$sec.$^{-1}$)	0.63×10^{-2}	0.25×10^{-2}	0.15×10^{-2}	0.11×10^{-2}	0.06×10^{-2}
u_a (m.sec.$^{-1}$)	23	17	13	11	9
c_D ($\times 10^3$)	3.8	2.0	1.6	1.3	1.0

Area averages (0-80 n.mi.):

$c_D = 1.7 \times 10^{-3}$

$Q_e/A = 1.0 \times 10^{-2}$ cal.cm.$^{-2}$sec.$^{-1}$ or 864 cal.cm.$^{-2}$ per day

$Q_s/A = 0.18 \times 10^{-2}$ cal.cm.$^{-2}$sec.$^{-1}$ or 155 cal.cm.$^{-2}$ per day

$r_B = 0.18$

B. August 27

$\rho = 1.15 \times 10^{-3}$ $T_0 = 28.0°C.$

	Radial Interval (n.mi.) 0-20	20-40	40-60	60-80
Q_a ($\times 10^{-12}$ cal.sec.$^{-1}$)	1.5	2.6	4.1	5.0
$T_0 - T_a$ (°C.)	2	2	2	2
$q_0 - q_a$ (g.kg.$^{-1}$)	3.9	4.0	4.5	4.8
r_B	0.20	0.20	0.18	0.17
A ($\times 10^{-14}$ cm.^{2})	0.43	1.29	2.15	3.01
Q_e/A (cal.cm.$^{-2}$sec.$^{-1}$)	2.91×10^{-2}	1.70×10^{-2}	1.62×10^{-2}	1.42×10^{-2}
Q_s/A (cal.cm.$^{-2}$sec.$^{-1}$)	0.58×10^{-2}	0.33×10^{-2}	0.29×10^{-2}	0.24×10^{-2}
v (m.sec.$^{-1}$)	41	32	29	25
c_D ($\times 10^3$)	2.6	2.0	1.8	1.7

Area averages (0-80 n.mi.):

$c_D = 1.9 \times 10^{-3}$

$Q_e/A = 1.65 \times 10^{-2}$ cal.cm.$^{-2}$sec.$^{-1}$ or 1425 cal.cm.$^{-2}$ per day

$Q_s/A = 0.29 \times 10^{-2}$ cal.cm.$^{-2}$sec.$^{-1}$ or 250 cal.cm.$^{-2}$ per day

$r_B = 0.18$

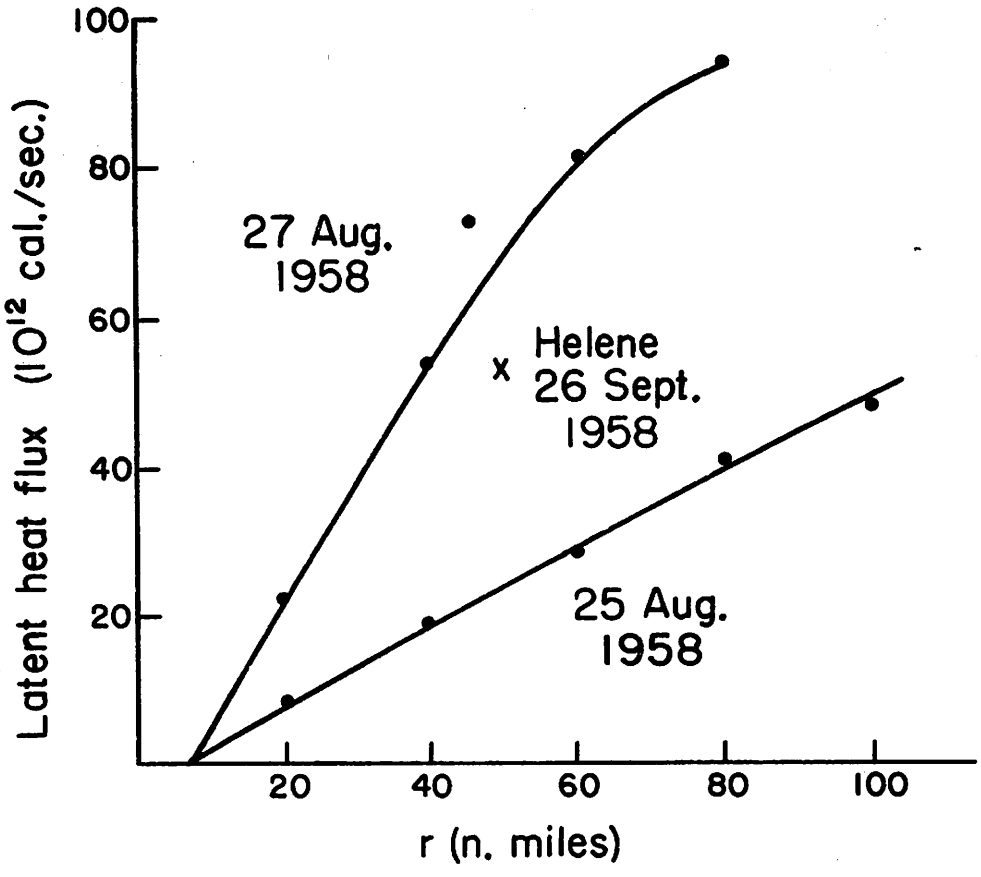

Figure 11. - Net latent heat import in troposphere as function of radius for Daisy August 25 and 27, also for Hene (September 1958) at the 50-mi. radius (denoted by the x).

of about 15 and 25, on the two days respectively. Even so, the oceanic source is still somewhat smaller than that predicted by Malkus and Riehl [19] for their model moderate storm. On the 25th, the net Q flux divergence was 55 percent that of the model, while it reached 78 percent on the 27th. Since Daisy's low-level winds (area-averaged 0-80 n.mi.) were on her maximum day only 66 percent of the model, and the remaining parameters entering the exchange computations were closely similar, the results of the comparison are consistent and encouraging.

4. THE MOISTURE BUDGET AND PRECIPITATION

The lateral component of the moisture flux divergence may be obtained from an equation like (5), neglecting the eddy term as found in table 1. Figure 11 shows the resulting net latent heat inflow, which is made up of a large import at low levels, and a very small export aloft.

To compute the precipitation within the storm core, we next convert the latent heat source to evaporation rate (table 3). It should be remembered here that evaporation is computed with respect to the storm center. Because of the storm's propagation, the evaporation from any given ocean area was, of

Table 3. - Moisture source

	Aug. 25	Aug. 27
Radius of area covered (n. mi.)	80	80
Total evaporative latent heat flux (x 10^{-12} cal. $sec.^{-1}$)	6.8	11.2
Evaporation depths ($cm.day^{-1}$)	1.4	2.3
Ratio of source to transport through boundary (percent)	18	12

course, less. Table 3 nevertheless indicates the magnitude of water loss to be expected from a fixed ocean area in case of a stationary storm. This is of particular interest with respect to the calculation for August 27 which shows that evaporation rose to high values as Daisy's intensity increased. Had the storm become stationary for a day, measurable cooling of the ocean might have occurred in view of the evaporation rate, hence the intensity of the hurricane would have been adversely affected.

Equation 4 may now be solved for the precipitation as a residual (fig.12). Both on August 25 and 27 the lateral gradient of precipitation was very large, as expected, and could be represented as a straight line on semi-logarithmic paper. In view of the rate of storm travel (average 6-7 kt.), a stationary rain gauge passed by the center would have collected 4-5 in. on August 25 and 12 in. on August 27. Neither amount is excessive, especially since the storm was rated by experienced meteorological observers of the research aircraft as a very "wet" one.

5. VERTICAL HEAT FLUX AND THE ROLE OF "HOT TOWERS"

Given the lateral heat transport of figures 9-10, vertical fluxes can be determined from continuity if there are no internal sources or sinks of Q. This is not quite true because of the radiation cooling. An estimate for the cooling of the whole mass has been obtained above, and it would be necessary to assign a vertical distribution of this cold source in order to include the heat sink for the vertical flux determination. This is difficult due to lack of knowledge about the radiation cooling as a function of height, and it is preferred to proceed without provision for radiation, especially as this would introduce only minor modifications.

In an analysis of the equatorial trough zone, Riehl and Malkus [29] separated the vertical heat flux into contributions by transport in "hot" cumulonimbus cores, by recycling in thunderstorm downdrafts, and by "diffusion" through smaller cumuli in the manner of the vertical heat flux in the trade-wind areas (Riehl et al. [24]). Since the air in the core of a hurricane is very moist throughout, a means for setting up strong downdrafts is lacking, and one would suppose that the second mechanism is negligible. If so, only the hot towers should be active above 500 mb., whereas lower down the smaller clouds may make a contribution in the layer where $\bar{Q}$ decreases upward, so that diffusion transports heat down the gradient.

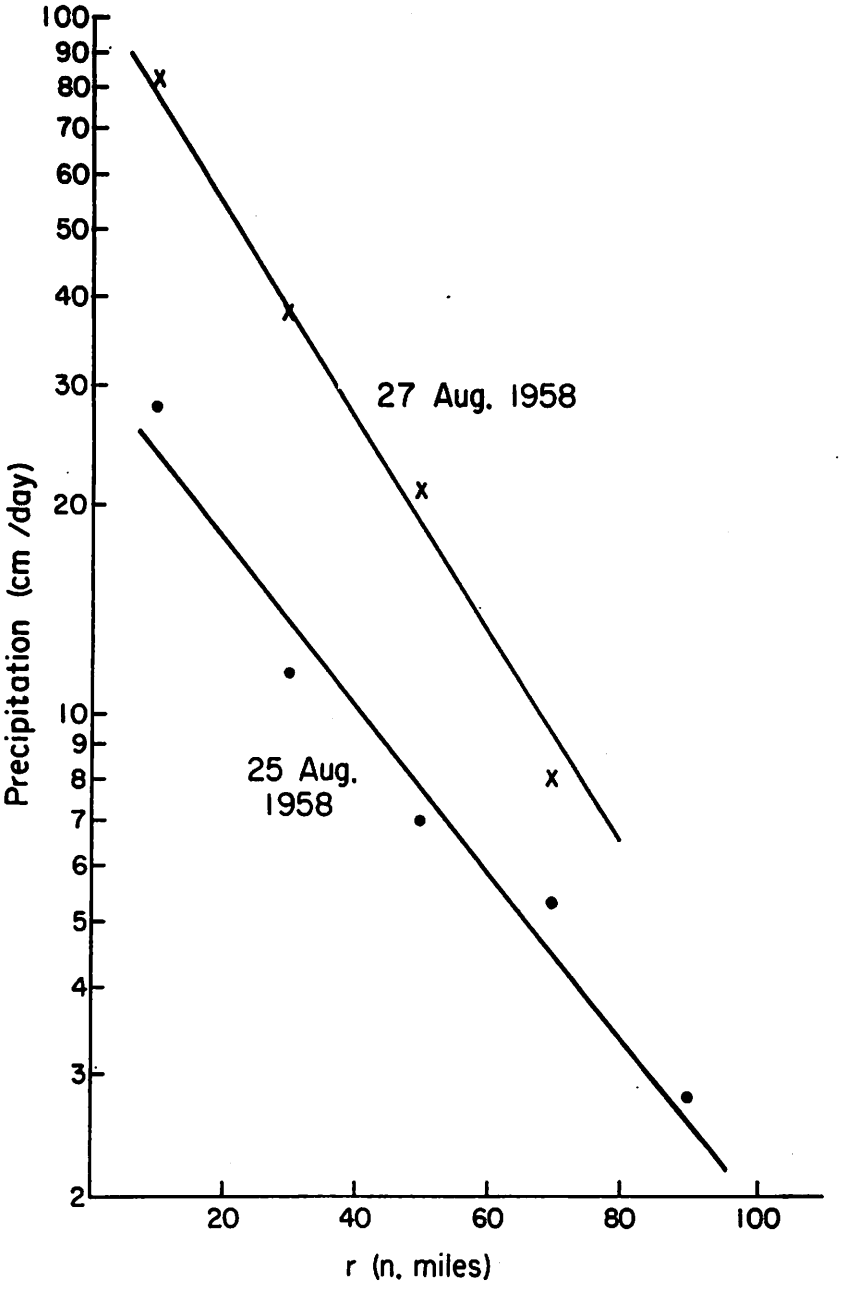

Figure 12. - Calculated radial distribution of precipitation for Daisy on August 25 and 27.

The vertical mass trasport M_z through a given isobaric surface may be divided

$$M_z = M_0 + (M_z - M_0) \tag{6}$$

where M_0 denotes the mass flux which has risen from the subcloud layer, presumably in hot towers, and $M_z - M_0$ is the mass which has entered from the sides above the top of the subcloud layer. Let Q_0 denote the heat content of

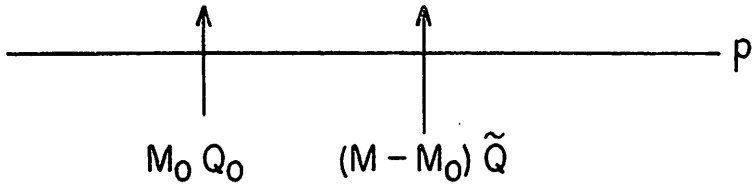

Figure 13. - Vertical heat flux mechanisms.

the air with characteristics of the subcloud layer and $\tilde{Q}$ the area-averaged heat content at any pressure surface. If all ascending mass not in hot towers has the heat content $\tilde{Q}$, and if internal sources and sinks are neglected, the vertical heat flux H_z through a given isobaric surface (cf. fig. 13) is

$$H_z = \bar{Q} M_z = M_0 Q_0 + (M_z - M_0)\,\tilde{Q} \tag{7}$$

Here $\bar{Q}$ is the mean heat content which must be possessed by M_z in order to accomplish the heat transport prescribed by figures 9-10. It can be computed from these diagrams and figures 5-6. Values of Q for August 25 are contained in table 4A; none of these computations was carried out for August 27 because of lower reliability of the deduced fluxes on that day.

Alternatively to equation (7), the vertical heat flux might also be expressed by

$$H_z = \tilde{Q} M_z + \widetilde{Q^o} M_z^o$$

where ^{o} denotes departure from the area average. As in the case of the equatorial trough study we prefer equation 6 to this formulation, because a transport $\tilde{Q} M_z$ does not occur at all and is merely a mathematical expression. We believe that equation (7) gives H_z in terms of components which have actual mechanistic existence.

Using mass continuity, we may solve equation (6) for M_0

$$M_0 = M_z \frac{\bar{Q} - \tilde{Q}}{Q_0 - \tilde{Q}} \tag{8}$$

At heights below the 500-mb. level this relation may be modified to allow for diffusion $Q^o M_z^o$ by the widespread smaller towers. Thus

$$\widetilde{Q^o M_z^o} = M_z \bar{Q} - M_0 Q_0 - (M_z - M_0)\,\tilde{Q} \tag{9}$$

for the lower layers. This relation can be evaluated if it is assumed that below the 500-mb. level there is no "erosion" of the hot towers; i.e. M_0 and $M_0 Q_0$ are constant between 900 and 500 mb. Table 4B-H shows the remainder of

Table 4. - Vertical heat flux calculations for August 25

Pressure(mb.)	Radial interval (n.mi.)				
	0-20	20-40	40-60	60-80	80-100
	A. $\overline{Q}$ (cal.g.$^{-1}$)				
200	83.4	82.9	83.4	82.0	82.0
300	83.0	82.5	82.6	82.0	82.0
400	82.5	81.6	81.5	81.3	80.5
500	82.4	81.4	81.2	81.0	80.2
600	82.6	81.6	81.2	81.1	80.2
700	83.3	82.0	81.4	81.2	80.5
800	84.7	82.7	82.0	81.5	80.6
900	89.5	85.6	83.7	82.4	80.7
	B. Q_0 (cal.g.$^{-1}$)				
Q_0	83.4	83.2	83.1	83.0	82.9
Area-averaged Q_0 = 83.2 cal.g.$^{-1}$					
	C. $\overline{Q} - \tilde{Q}$ (cal.g.$^{-1}$)				
200	0.85	0.6	1.3	0	0.1
300	1.6	1.4	1.7	1.3	1.3
400	1.5	0.9	1.3	1.4	0.8
500	1.5	0.8	1.0	1.2	0.6
600	2.0	1.0	1.0	1.1	0.4
700	2.4	1.4	1.1	1.0	0.4
800	3.8	2.0	1.5	1.1	0.3
900	8.1	4.4	3.0	1.7	0.2
	D. $Q_0 - \tilde{Q}$ (cal.g.$^{-1}$)				
200	0.85	0.9	1.0	1.0	1.0
300	2.0	2.1	2.2	2.3	2.2
400	2.4	2.5	2.9	3.1	3.2
500	2.5	2.6	2.9	3.2	3.3
600	2.7	2.7	2.9	3.0	3.1
700	2.5	2.6	2.8	2.8	2.8
800	2.5	2.5	2.6	2.6	2.6
900	2.0	2.0	2.5	2.3	2.4
	E. Fraction of vertical mass flux in hot towers $(\overline{Q} - \tilde{Q})/Q_0 = Q$				
200	1.00	0.67	1.0	0	0.10
300	0.80	0.67	0.77	0.57	0.59
400	0.63	0.36	0.45	0.45	0.25
500	0.60	0.31	0.35	0.38	0.18

Table 4. - Continued

Pressure(mb.)	Radial interval (n.mi.) 0-20	20-40	40-60	60-80	80-100
F. Mass flux rising in hot towers M_0 (10^{11} g.sec.$^{-1}$)					
200	2.1	0.9	3.2	0	negligible
300	6.7	4.9	4.9*	4.8	2.5*
400	6.7	4.9	4.9*	5.6*	2.0*
500	6.7	4.9	4.6	5.5	1.9
900-500	6.7	4.9	4.6	5.5	1.9
M_0/A(900-500) (gm.cm.$^{-2}$)	15.6×10^{-3}	3.8×10^{-3}	2.1×10^{-3}	1.8×10^{-3}	0.5×10^{-3}

*Values slightly in excess of those for layer 900-500 mb. indicate limit of computational reliability.

G. Percent of vertical heat flux carried by hot towers

$$\frac{M_0 Q_0}{M_z Q} = \frac{M_0 Q_0}{H_z}$$

Pressure(mb.)	Radial interval (n.mi.) 0-20 Percent	20-40 Percent	40-60 Percent	60-80 Percent	80-100 Percent	Mean Percent
200	100	67	98	0	0	
300	82	71	79	62	62	71
400	66	41	52	50	30	48
500	65	36	42	45	23	42
Mean	78	54	68	*52	*38	

*Omitting 200-mb. level

H. Vertical mass flux not in hot towers $M_z - M_0$ (10^{11} g.sec.$^{-1}$)

Pressure(mb.)	Radial Interval (n.mi.) 0-20	20-40	40-60	60-80	80-100
200	0	0.5	0	1.0	0.5
300	1.7	2.4	1.5	3.6	1.8
400	4.1	8.8	5.9	7.1	6.2
500	4.5	10.8	8.4	8.9	8.4
600	3.1	9.8	8.3	8.9	8.4
700	1.0	7.0	6.9	8.2	7.4
800	*	3.2	4.0	5.8	5.7
900	*	*	*	1.2	2.6

*Active turbulent diffusion

the calculations for August 25. We see that $\bar{Q} - \tilde{Q}$ is positive throughout, as expected (table 4C). Furthermore $Q_0 > \bar{Q}$ everywhere except at 800 and 900 mb. at the inner wall and at 900 mb. in the intervals 20-40 and 40-60 n.mi. (table 4A, B). This indicates that diffusion is very active up to about 700 mb. near the eye and up to 850 mb. a little farther out. Beyond this convective core and above 700 mb. near the eye $\overset{\circ}{Q}\overset{\circ}{M}_z$ proved negligible.

The ratio $M_0/M_z = (\bar{Q} - \tilde{Q})/(Q_0 - \tilde{Q})$ in table 4E is somewhat irregular but in general decreases outward, as expected. Although the irregularities may arise from our data, sampling, and computational deficiencies there was a clear suggestion in the cloud mapping (Malkus et al.[20]) that within the core ($r < 100$ n.mi.) convective activity was highly concentrated in the eye wall and again at about 60 n.mi., with more tower-free spaces intervening. M_0 itself shows a rather uniform distribution with radial interval out to 80 n.mi.; however, the last line in table 4F shows that per unit surface area, hot tower mass ascent was fantastically concentrated in the innermost core. Along the vertical, M_0 remained closely constant in view of the buoyancy in the cumulonimbus cores which permits the mass to ascend rapidly without much lateral mixing. In contrast, the mass flow $M_z - M_0$ (table 4H) with less buoyancy, could not penetrate to the high troposphere; in fact, it diminished immediately above the level of non-divergence near 500 mb. In consequence of this distribution, the percentage of H_z carried by the hot towers increases upward and decreases outward (table 4G). The hot cores thus play an ever-increasing role as the center is approached, and they furnish the primary mechanism for heat flux to the high troposphere. Nevertheless, there was no requirement on August 25 that all rising mass go up in hot towers, nor was there any need to introduce recycling. It may be suggested that the potential intensity of a hurricane is related to the fraction of M_z channelled through the hot towers and its current intensity to the magnitude of M_0. These points are pursued in the following sections.

Number of hot towers: We may now compare the mass flux requirements in hot towers (table 4F) with the observed number penetrating the upper NHRP flight level (237 mb. or about 37,000 ft.) and with computations on the dynamics of individual cumulonimbus in Daisy.[1] From the latter, the ascent rate at this level of a buoyant element 4 km. in diameter was about 12 m.sec.$^{-1}$ The photographs discussed by Malkus et al. [20] and other evidence gave this as the typical horizontal dimension of the penetrative towers on the 25th.

The upward mass flux through 237 mb. effected by one hot tower M_T with an area A_T, density ρ_T, and rising at a rate W_T therefore is

$$M_T = \rho_T A_T W_T \cong 6 \times 10^{10} \text{ g.sec.}^{-1}$$

---

[1] Some of these calculations (for August 27) have been published by Malkus [18]. Similar calculations for the 25th, quoted here, are unpublished at the present time.

where $\rho_T \approx 0.4 \times 10^{-3}$ g.cm.$^{-3}$. From table 4F, the total mass flux M_0 within 100 n.mi. is about 15×10^{11} g.sec.$^{-1}$ which means that 25 active hot towers at a time are required within the storm core. The film measurements gave about 60 within 200 n.mi., so that the agreement could hardly be better, allowing for the fact that some of the towers photographed had ceased their actively rising phase when counted.

It is also significant to note that, within 100 n.mi. on the 25th, the total mass in hot towers rising through the 500-mb. level was 23.6×10^{11} g. sec.$^{-1}$ or within computational error of the lateral mass inflow in the layer 1000-900 mb. at the 100 n.mi. boundary (22.0×10^{11} g.sec.$^{-1}$ from fig. 5). We suggest the correspondence between supply of subcloud air and hot tower ascent; this is supported by evidence on August 27. By the mature day, inflow (at 80 n.mi.) in the 1000-900 mb. layer had increased over the 25th by a factor of 56.7/17.5 = 3.25, while the number of penetrative hot towers within 200 n.mi. was assessed from the photographs as about 200, or an increase of a factor of 3.3 over the 25th! We shall explore some further aspects of the relationships of hot towers to hurricane development and maintenance in the next section on ventilation.

6. VENTILATION

Early computations of the mean wind distribution in tropical storms at upper levels (E. S. Jordan [13]) indicated that $\bar{v}$ vanishes a few thousand feet above the surface, so that most inflow takes place in the subcloud layer. Later computations of the average wind field in Atlantic hurricanes (Miller [21]) and of several but not all individual cases from research flight information (Simpson and Riehl [30]; Gangopadhyaya and Riehl [5]) as well as figures 5 and 6 of this article, have shown that finite values of $\bar{v}$ can occur well above the subcloud layer and that the maximum inflow on occasion was situated as high or higher than the 700-mb. level, at least at a radius of several hundred miles. Since Q decreased above the subcloud layer in every case investigated, such radial motion introduces lower values of Q (lower temperature and/or lower humidity, mainly the latter) into a hurricane or tropical depression, thus acting as a constraint on hurricane formation and maintenance.

This advection, called <u>ventilation</u>, may be defined for symmetrical circulations by

$$V_e = M_i(Q_i - Q_0) \tag{10}$$

where M_i is the lateral inflow above the mixed layer and Q_i is its heat content. The principle of conservation of energy may be written for a volume as depicted in fig. 14

$$M \frac{\partial Q^*}{\partial t_R} = M_0 Q_0 + \sum^{n} \Delta M_i Q_i - \sum^{m} \Delta M_u Q_u \tag{11}$$

where M is mass and use has been made of mass continuity in the form

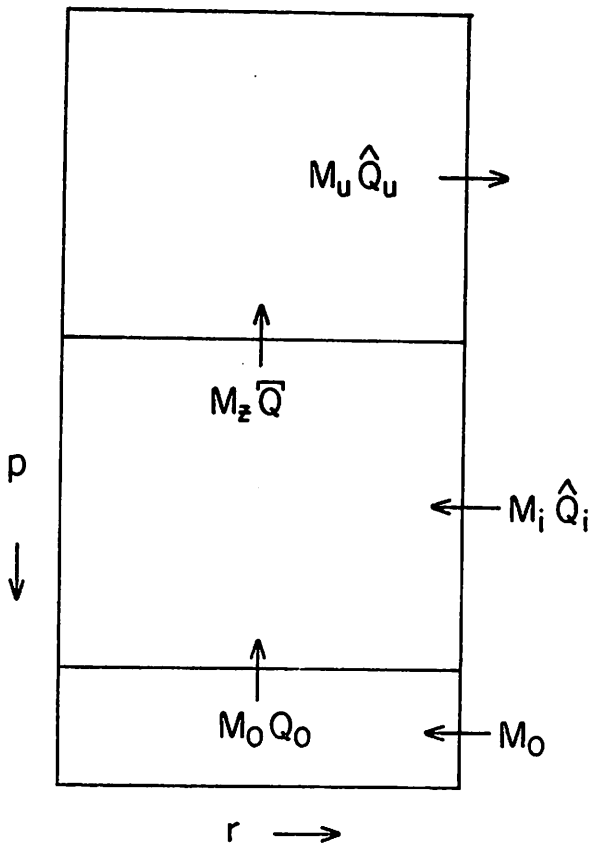

Figure 14. - Illustrating ventilation schematically.

$$M_0 + \sum^{n} \Delta M_i = \sum^{m} \Delta M_u = M_u$$

where the subscripts i and u denote inflow and the summations are made (generally at 100-mb. intervals) over the inflow and outflow layers, respectively. At the 900-mb. level we shall assume undiluted upflow at the heat content of the air in the mixed surface layer, which may include contributions by the local oceanic heat source. Analogous to equation (7) we define

$$\sum^{n} \Delta M_i Q_i = M_i \hat{Q}_i$$

$$\sum^{m} \Delta M_u Q_u = M_u \hat{Q}_u$$

Then

$$M \frac{\partial Q^*}{\partial t_R} = M_0 Q_0 + M_i \hat{Q}_i - M_u \hat{Q}_u \qquad (12)$$

Ventilation may be introduced explicitly by adding and subtracting the identity (10). Then

$$M \frac{\partial Q^*}{\partial t_R} = M_u (Q_0 - \hat{Q}_u) + M_i (\hat{Q}_i - Q_0) \qquad (13)$$

The criterion for the growth of the disturbance is

$$\frac{M_i}{M_u} \gtrless \frac{Q_0 - \hat{Q}_u}{Q_0 - \hat{Q}_i} \qquad (14)$$

For example, given $Q_0 - \hat{Q}_u = 1$ cal.g.$^{-1}$ and $Q_0 - \hat{Q}_i = 2$ cal.g.$^{-1}$, then the disturbance will grow if $M_i/M_u < 0.5$. From boundary observations all values are given except Q_0 which, when a large boundary such as the 5° radius is considered, may be taken as the heat content of the inflowing trade-wind air. In case of large mid-tropospheric inflow at the usual minimum of Q_i there, ventilation must act to weaken a storm.

For Daisy, the complete information is already contained in figures 9 and 10 and indeed the computation from equation (14) does not add to this information, but merely helps to establish a simple picture. We find that $M_i/M_u = 0.65$ at the 100 n.mi. radius on August 25; further $\hat{Q}_i = 80.1$ and $\hat{Q}_u = 81.2$ cal.g.$^{-1}$ If the surface value of 83.2 cal.g.$^{-1}$ is used for Q_0 at 900 mb., then $(Q_0 - \hat{Q}_u)/(Q_0 - \hat{Q}_i) = 0.65$. Within the limits of the computation, the equal sign of equation (14) applies. This shows there is at least no tendency for the environment to suppress the developing storm. Given an oceanic heat source, it can maintain the existing circulation against radiation and provide for some heat export and internal increase of heat content with time.

It is probable that the main utility of the ventilation calculation, as formulated here in equation (14), lies in applying it at an outer radius, say 300 n.mi., to potentially formative situations. This will indicate whether internal heating is strongly hindered. Given a mature hurricane, it will show whether weakening is likely to set in through increase of ventilation across the boundary of the calculation. In the case of Daisy where core data were available, we may explore the effects of ventilation in more mechanistic detail.

Table 5A shows the individual terms in equation (11) for the 25th (boundary 100 n.mi.) and for the 27th (80 n.mi.). On the former day we took Q_0 and M_0 from table 4, and on the latter day Q_0 was assumed as 84.0 cal.g.$^{-1}$ (see Appendix table 8) and M_0 was taken as equal to the lateral boundary inflow between 1000 and 900 mb. On the 25th, the storm was gaining ground; the net warming (ignoring radiation) is comparable to the oceanic source. On the 27th, it was barely holding its own.

We may next inquire what degree of constraint upon Daisy's potential development was imposed by ventilation. It is interesting to note from figure 6 that on the mature day the total mass inflow at 80 n.mi. was almost exactly equal to that of the model moderate hurricane of Malkus and Riehl [19] and yet the winds, eye-wall surface pressure, and oceanic source fell somewhat short

Table 5. - Ventilation

A. Effect upon heat budget

Date	$M\partial Q^*/\partial t_R$	$M_0 Q_0$	$\sum M_i Q_i$	$\sum M_u Q_u$
		Unit: 10^{12} cal.sec.$^{-1}$		
Aug. 25 - Actual	+ 11.8	196.3	340.4	524.9
Aug. 25 - No ventilation	+ 26.9	550.8	-	524.9
Aug. 27 - Actual	- 0.5	476.3	486.5	963.3
Aug. 27 - No ventilation	+ 20.7	984.0	-	963.3

B. Parameters and comparisons

	Aug. 25	Aug. 27
Boundary radius (n.mi.)	100	80
$\tilde{Q}_0$ (cal.g.$^{-1}$)	83.2	84.0
M_0 (g.sec.$^{-1}$)	23.6×10^{11}	56.7×10^{11}
Increase in M_0 for no ventilation (percent)	280	107
Increase in Q_a for no ventilation (percent)	18	41

of those they calculated. In the model ventilation was not considered, the entering mass all arrived in the layer 1000-900 mb., and the vertical soundings at each radius were governed by wet-adiabatic ascent of subcloud air. Therefore the hypothetical computation in table 5A was carried out; it places all Daisy's inflow in the layer 1000-900 mb. and raises it in hot towers M_0 with heat content Q_0, leaving the outflow unaltered. To raise the heat content of the additional inflow from its subcloud values at the boundary to Q_0 would require an enhanced oceanic source of only 18 percent on the 25th, but of 41 percent on the 27th.

Since the rate of warming $M\partial Q^*/\partial t_R$, is more than doubled by this alteration on the 25th, and raised from a slight cooling to a significant warming on the 27th, one might infer that Daisy would have become an extreme storm, were only the constraint of ventilation removed. This, however, is not quite the case.

Malkus and Riehl showed that the intensity of a hurricane is proportional to the excessive heat content of the air rising in the inmost core. On August 25-27, Daisy's vertical sounding at 20 n.mi. radius was somewhat cooler than prescribed by adiabatic ascent of surface air, due to introduction of the

ventilation inflow at mid-levels. Thus, to assess how deep Daisy would have been without ventilation, we made hydrostatic computations at the 20 n.mi. radius assuming now an undilute wet-adiabatic sounding at the heat content Q_0 for each day. On the 25th, the surface pressure could have been lowered 10-12 mb. by removal of the Q_1 air and substitution of undilute ascent, while for the 27th the figure is about 8-10 mb.

Using the dynamic relationships of the model, we find that on the 25th, this lowering of eye-wall pressure and the accompanying increase of wind speed would readily have enhanced the oceanic source more than the 18 percent required to maintain the new subcloud inflow at the 25th Q_0, thus allowing Q_0 to increase further and the storm to continue deepening, while this was not so on August 27th. On the 27th, lowering of the eye-wall pressure by 8-10 mb., or to the values for the model moderate storm, would have increased the inner wind to about 57 $m.sec.^{-1}$, or again just comparable to the model. With the prevailing air-sea temperature difference, this wind increase would have permitted the oceanic source to become just marginally large enough to maintain the new status quo. In fact, the work of Malkus and Riehl (equation (42),[19]) suggests that the upper limit of development has been reached for this air-sea property difference when innermost pressures are to be maintained by ascent of subcloud air.

Thus while ventilation prevented Daisy from quite realizing its full potential, which was approximately that of the model moderate storm, it cannot be offered as the reason the storm did not achieve extreme intensity. To do that, it would have had either to move over warmer water or been able to lower the core pressure by some other means than hot tower ascent only, such as perhaps by an eye wall slanting outward over the inner rain area. We may suggest, however, that ventilation may be the critical inhibitor in the development in many or most cases from tropical disturbance to model moderate hurricane. Whether a storm like Daisy could have continued to intensify beyond August 25 had it not been able to concentrate an increasing percentage of inflow in the subcloud layer, and what permitted it to do this where other storms fail are questions we raise for further hurricane research to explore. We turn next to the motion field and kinetic energy budgets of Daisy as they were actually observed.

7. THE KINETIC ENERGY BUDGET

The kinetic energy equation may be written

$$\rho \frac{dK}{dt} = -g\rho \mathbb{V} \cdot \nabla D + \mathbb{V} \cdot \frac{\partial \boldsymbol{\tau}}{\partial z} \qquad (15)$$

Here K is kinetic energy per unit mass, ρ density, $\mathbb{V}$ the horizontal vector wind and $\boldsymbol{\tau}$ the horizontal shearing stress vector. Further, it has been assumed that all dissipation of kinetic energy takes place by vertical turbulence, an assumption which will be examined further below. Equation (15) will be integrated over a volume α between two concentric cylinders with use of mass continuity. In the integration of the frictional term it will be assumed that $\boldsymbol{\tau} = \mu \frac{\partial \mathbb{V}}{\partial z}$, where μ is the coefficient of turbulent mass

exchange, and that at ship's deck level $\tau_0 = c_D \rho_0 \mathbb{V}_0 V_0$ where c_D is the drag coefficient, $\mathbb{V}_0$ is the vector wind and V_0 its magnitude at this level. Then

$$M \frac{\partial K^*}{\partial t_R} = - \int_\sigma K \rho c_{nR} \, d\sigma - \int \mathbb{V} \cdot \nabla D \, dA \, dp - c_D \rho_0 \tilde{V}_0^3 A - \int_\alpha \mu \left(\frac{\partial V}{\partial z}\right)^2 d\alpha, \tag{16}$$

if there is no transfer of kinetic energy through the top of the storm by shearing stresses and the turning of wind with height is small through the bulk of the hurricane.

Local change: The total kinetic energy was 0.6×10^{14} kj. inside the 80-mi. radius on August 25 and 1.3 such units on August 27. Since the flight data for August 28 indicate that the storm was still growing in energy between the 27th and 28th, a uniform growth rate of 0.4×10^{14} kj.day^{-1} will be used. This corresponds to 0.46×10^9 kj.sec.$^{-1}$ or 0.1×10^{12} cal.sec.$^{-1}$ in heat units; about an order of magnitude less than $M \frac{\partial Q^*}{\partial t_R}$ which itself could be neglected compared to the heat transports and sources. Such a situation is usually found in energy budget calculations. It must nevertheless be recognized that it is this very small increment which is of greatest interest in hurricanes.

Kinetic energy advection: The transport of kinetic energy by the mass circulation $\bar{K} M_r$ is readily determined from vertical profiles of $\bar{K}$ and the mass flow. But the contribution due to $V_R' K'$ is difficult to assess because of the few flight levels and data uncertainties. Table 6 shows the available "eddy" transports. They are irregular in sign on the 25th and much smaller than on August 27, wnen this transport was directed outward at both flight levels, especially in the high troposphere. This suggests that the mass outflow took

Table 6. - Eddy transport of kinetic energy, 10^7 kj.sec.$^{-1}$ 100 mb.$^{-1}$

		Radius (n.mi.)			
		20	40	60	80
Aug. 25:	237 mb.	- .2	-4	- .2	1.9
	560 mb.	- .7	-3.5	- .3	-1.7
	810 mb.	- .9	1.7	2.9	-1.2
Aug. 27:	247 mb.	1.9	14.2	23.2	31.0
	630 mb.	9.9	11.0	10.1	14.4

place in organized channels of relatively high speed. In order to obtain values integrated over the troposphere some assumptions must be made. On August 25 the arithmetic mean of the three flight levels was taken and applied to a layer of 800-mb. thickness. On August 27 the values measured at 247 mb. were applied to a layer of 200-mb. thickness and those measured at 620 mb. to a layer of 600-mb. thickness.

Table 7 summarizes the kinetic energy transports. Flux due to mass circulation increased by an order of magnitude between the two days, largely because of the increase in mass circulation itself. On August 25 the "eddy" transport was only a small fraction of that due to the mean circulation and is best neglected, especially in view of the irregular distribution of signs in Table 6. On August 27, however, the "eddy" flux was about 25 percent of the mean flux at all radii, and it opposed the transport by the mean circulation. This contribution will be retained. But the limitations of the whole calculation in tables 6 and 7 are evident.

Kinetic energy source: In determining the source term only the contribution by the mass circulation was evaluated. This term is readily computed within the limits of accuracy of the mass circulation. Since the contours of the isobaric surfaces formed nearly concentric circles, the contributions by $\overline{V'_R \frac{\partial D'}{\partial r}}$ and $\overline{u' \frac{\partial D'}{r \partial \theta}}$ most likely were small. Thus, $-\int \mathbb{V} \cdot \nabla D dA dp = -\int \bar{v} \frac{\partial \bar{D}'}{\partial r} dA dp$.

The distribution of $\bar{D}$ is shown in figure 15 for August 25. As would be expected in a warm-core vortex, the negative $\bar{D}$'s (as also $\frac{\partial \bar{D}}{\partial r}$) decreased upward and outward. In the high troposphere the D-gradient was directed outward beyond the 50-mi. radius. Thus the main seat of kinetic energy production was in the low levels where the mass flows in and the D-gradient was large. In the layer 500-300 mb., and in the upper troposphere inside the 50-mi. radius, the outflow did work against the pressure field. But, since the D-gradient was small here compared to the low levels, the kinetic energy sink was much smaller than the source. Beyond the 50-mi. radius, the circulation acted to generate kinetic energy at almost all heights.

Tables 8-9 contain the kinetic energy budget. For August 27 four 20-mi. intervals are shown. On August 25 values were somewhat more irregular, presumably because all energy transformations were much smaller; it is preferred to show only two radial intervals, for the inner and the outer region. The unit chosen is 10^{14} kj. so that the transformations may be compared with total kinetic energy inside the 80-mi. radius ($\sim 1 \times 10^{14}$ kj.). Signs have been chosen so that the positive sign denotes a contribution toward increasing kinetic energy. The line marked "local change" refers to the change with respect to the moving system as defined above. Evidently this term is very small, and essentially we deal with a balance between production and advection on one hand, and frictional dissipation on the other.

From tables 7-9 all terms, except the time change, have the magnitude of total kinetic energy after integration over a day; on the 27th, in fact, the total energy is replaced completely every 2 to 3 hours. This helps to explain why the energy of hurricanes runs down very quickly in the inner core after they strike land.

Table 7. - Kinetic energy transport (10^{17} ergs $sec.^{-1}$)

		Radius (n.mi.)			
		20	40	60	80
Aug. 25:	$\bar{K}\,\bar{v}\ 10^7$ kj.$sec.^{-1}$	- 18.3	- 23.1	- 26.5	- 25.0
	$\overline{K'v_R'}\ 10^7$ kj.$sec.^{-1}$	- 4.0	- 4.8	- 4.8	- 3.2
	Total 10^{14} kj.day^{-1}	- 0.2	- 0.2	- 0.2	- 0.2
Aug. 27:	$\bar{K}\,\bar{v}\ 10^7$ kj.$sec.^{-1}$	-248	-394	-490	-496
	$\overline{K'v_R'}\ 10^7$ kj.$sec.^{-1}$	64	94	106	149
	Total 10^{14} kj.day^{-1}	- 1.6	- 2.6	- 3.3	- 3.0

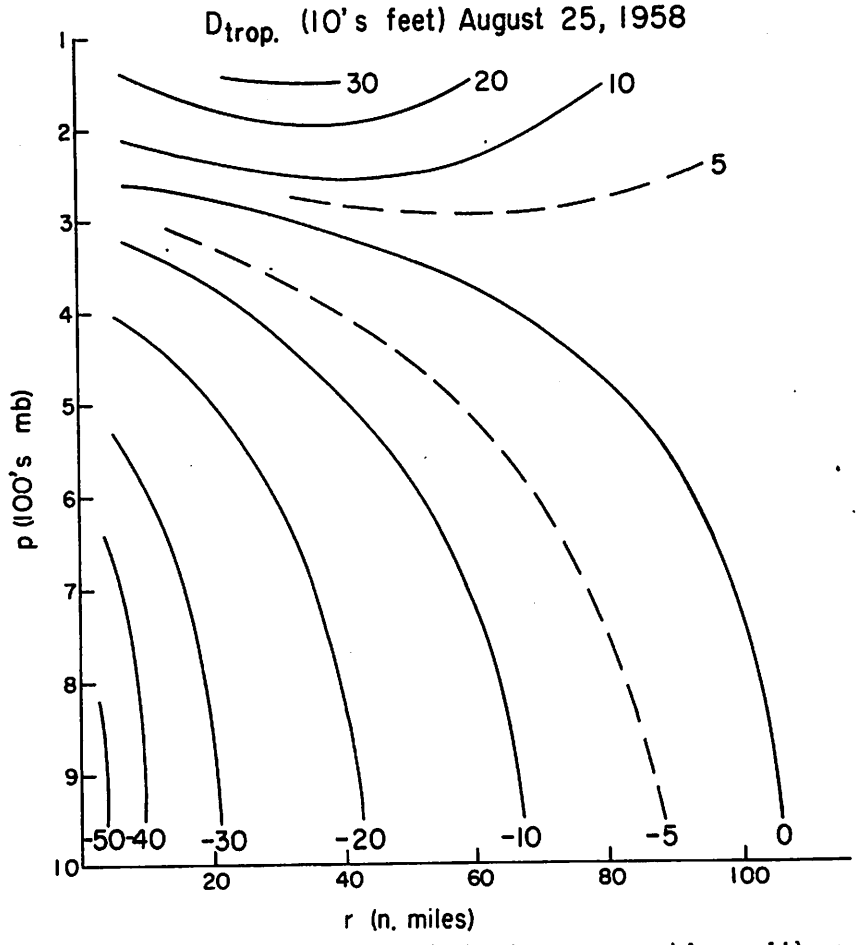

Figure 15. - Vertical cross section of altimeter correction with respect to the mean tropical atmosphere on August 25.

Table 8. - Kinetic energy budget August 25 (10^{14}kj.day^{-1})

	Radius (n.mi.)		
	0-40	40-80	0-80
Advection	.20	.02	.22
Production	1.06	1.34	2.40
Local change	.13	.22	.35
Ground dissipation	.57	.81	1.38
Advection plus production	1.26	1.36	2.62
Local change plus ground dissipation	.70	1.03	1.73
Left over for internal friction	.56	.33	.89
Ratio of internal to ground friction	1.0	.4	

Table 9. - Kinetic energy budget August 27 (10^{14}kj.day^{-1})

	Radius (n.mi.)				
	0-20	20-40	40-60	60-80	0-80
Advection	1.6	1.0	.7	- .3	3.0
Production	1.0	2.0	1.5	1.4	5.9
Local change	.1	.1	.1	.1	.4
Ground dissipation	.6	.8	.7	.7	2.8
Advection plus production	2.6	3.0	2.2	1.1	8.9
Local change plus ground dissipation	.7	.9	.8	.8	3.2
Left over for internal friction	1.9	2.1	1.4	0.3	5.7
Ratio of internal to ground friction	3.2	2.6	2.0	.4	

On August 25 advection contributed little to storm growth and maintenance. Transport through the 80-mi. radius was negligible, so that in this development stage the production mechanism in the interior was all-important. On the 27th, transport through the 80-mi. radius contributed no less than three units, which is an order of magnitude larger than on August 25. From table 9, the maximum transport actually occurred near the 60-mi. radius. Thus the energy imported was made available almost wholly to the inner zone.

In contrast to the large increase in advection, production inside the 80-mi. radius merely doubled between the two days. Hence energy production shifted outward as the storm grew, since presumably the three units advected toward the core were generated mainly within the peripheral circulation. For comparison, Palmén and Riehl [22] computed 4.1 units for production inside the 120-mi. radius for the mean hurricane, a value closer to Daisy on the 25th than on the 27th. All interest now turns on the question of the disposal of the large amount of energy produced within the storm and imported toward its core.

Dissipation in the surface boundary layer: From equation (16) the dissipation of kinetic energy in the surface boundary layer is proportional to V_0^3 averaged over the area of calculation. This quantity was not available on either day, and in fact it cannot be obtained from aircraft missions. Various studies of upper winds, based on radio-wind and pilot balloon observations, have indicated that V varies little with height from the surface to the middle troposphere. Palmén and Riehl [22] actually assumed a slight decrease of wind speed from 950 mb. toward the ocean. For determination of ground friction in Daisy, uniform speed from the lowest flight level down was postulated. On August 25 the legs at 960, 915, 830, and 560 mb. support this assumption quite well. On August 27, the 620-mb. level was the lowest one flown, and the wind field observed there must be assumed to be representative also of surface conditions.

An assumption must also be made about the drag coefficient, a subject discussed by Palmén and Riehl and in Section 3 herein. The dependence of c_D on wind speed, sea condition, and other parameters is a difficult topic and is not yet solved satisfactorily especially for high wind speeds. In view of the somewhat low values found for Daisy in table 2 and the uncertainties in its calculation, a uniform value of $c_D = 2.5 \times 10^{-3}$ was used in the energy and momentum budgets, as the most probable value from previous investigations. Should this procedure have been incorrect, it will be necessary to revise the ground dissipation in tables 8-9 downward substantially. It appears certain, at least, that this term has not been underestimated.

Granted the general accuracy of the ground dissipation calculation, it is of interest that on August 27, and to a lesser degree on August 25, this dissipation was nearly independent of the radius. Thus

$$V_0^3 \, r^2 = \text{const} \qquad (17)$$

for constant c_D. Malkus and Riehl [19] found a similar distribution in a semi-theoretical model. For a symmetrical vortex equation (17) becomes

$$V_0 r^x = V_0 r^{.66} = \text{const.} \qquad (18)$$

Many calculations of the exponent x in equation (18) have been made in the literature. Values between 0.5 and 0.6 have given good fit in a large number of cases. In Daisy x = 0.55 verifies for August 27. Since

$\overline{V_0^3} > \bar{V}_0^3$, a coefficient somewhat lower than that computed for the symmetrical vortex should be expected; the range 0.5 to 0.6 appears excellent. Thus there is a suggestion of a general law in hurricanes: that dissipation of kinetic energy in the surface layer is independent of distance from the center.

Internal friction: The most spectacular result of tables 8 and 9 is the large residual imbalance which developed between our two days and which must be attributed to a great increase in internal friction. For the general circulation it has been estimated that internal and ground dissipation may be equal. This value was not exceeded on August 25 when, also, the ratio of internal to ground friction decreased outward strongly as would be expected from the radial distribution of turbulence elements.

On August 27 the ratio decreased outward as on August 25 and was reduced to the same magnitude beyond the 60-mi. radius. In the inner zone the calculated values are so strong (though well in keeping with the character of the type of circulation investigated) that the result must be considered as quite tentative. Extensive investigation of other cases plus further observations are requisite for confirmation. It is of interest, however, that the problem of disposal of kinetic energy generated also arose in the hurricane model of Malkus and Riehl [19]. In the kinetic energy budget (fig. 9 of their report) the ground dissipation is comparable to that of August 27. Balance is made in the lowest kilometer (the sole object of that study) by upward transport. If the computations had been extended higher up, import plus production by pressure forces would have had to be balanced by internal dissipation, and it is likely that the required magnitude would have been as large as on August 27.

Thus the semi-theoretical work predicted the difficulty encountered in Daisy. The possibility exists that an important contribution may be made here toward understanding the limits of wind speeds attained in hurricanes by means of a constraint which grows in relative importance with the storm. In the following, possible mechanisms for achieving the internal dissipation will be taken up.

Dissipation may be accomplished by vertical and/or lateral eddies within the hurricane structure. An attractive possibility exists along the vertical. As discussed above and also by Malkus et al.[20] in the cloud study of Daisy, most ascent is likely to have taken place in narrow towers covering only a few percent of the area. The vertical velocity then is large (fig. 7) and individual elements may be expected to reach the high troposphere with little loss of kinetic energy. In spite of the sampling difficulties, the high-level NHRP aircraft encountered speeds near 80 kt. in Daisy and 95 kt. in Helene of 1958 at 240 mb. on just a few passes. These high-wind areas were very localized. The suggested picture is that the high-energy stream reaches the upper troposphere in narrow columns and then is brought rapidly in contact with

environmental air which has already lost its energy by mixing and motion toward higher pressure. In the course of this contact the high energy of the fresh stream is given up to the low-energy surroundings, and this may be the mechanism of the internal dissipation process. If so, an Austausch coefficient of 10^3 g.cm.$^{-1}$sec.$^{-1}$ would be required in view of the existing shears, if one wishes to apply this form of turbulence expression. The value is not excessive under the circumstances, especially when it is considered that Riehl et al.[26] required a coefficient of 500 g.cm.$^{-1}$sec.$^{-1}$ for momentum balance of the average trades in the northeastern Pacific Ocean.

On account of the uniformity of wind with height below 500 mb., the dissipating mechanism just outlined may not be important there. Yet the small-scale wind fluctuations are such that judgment must be reserved. It should be added that Gray[7] has computed strong frictional forces in the low and middle troposphere in dynamical calculations.

Considering next the possibility of lateral stresses, we shall investigate the radial stress of the tangential wind which is likely to make the largest contribution. This stress

$$\tau_{\theta r} = \mu_r \left(\frac{\partial u}{\partial r} + \frac{u}{r}\right),$$

and its radial derivative

$$\frac{\partial \tau_{\theta r}}{\partial r} = \mu_r \left[\frac{\partial^2 u}{\partial r^2} + \frac{1}{r}\frac{\partial u}{\partial r} - \frac{u}{r^2}\right] = \mu_r \frac{\partial \zeta_\theta}{\partial r}, \qquad (19)$$

where μ_r is the lateral exchange coefficient for momentum and ζ_θ is the relative vorticity of the tangential wind. Dissipation of kinetic energy by internal friction (IF) of this character

$$IF = \iint \frac{\mu}{\rho}\frac{\partial \zeta_\theta}{\partial r}\, u\, dA\, \frac{dp}{g} \qquad (20)$$

This formula was evaluated assuming μ_r independent of height and neglecting the horizontal correlations of $\frac{\partial \zeta_\theta}{\partial r}$ and u which may be a substantial omission. However, only an order of magnitude estimate is wanted for comparison with previous calculations. Defant [4] estimated the coefficient of latitudinal turbulent mass exchange to be 5×10^7 g.cm.$^{-1}$sec.$^{-1}$ for the heat balance of the general circulation, and Grimminger [8] obtained 4×10^5 to 5×10^7 from the spread of moisture on isentropic charts. If the order of magnitude of A and μ in lateral turbulence is the same, then μ_r between 10^5 and 10^7 would be reasonable. Table 10 contains the calculated coefficients for August 25 and 27, where a uniform density of 10^{-3} g.cm.$^{-3}$ has been used.

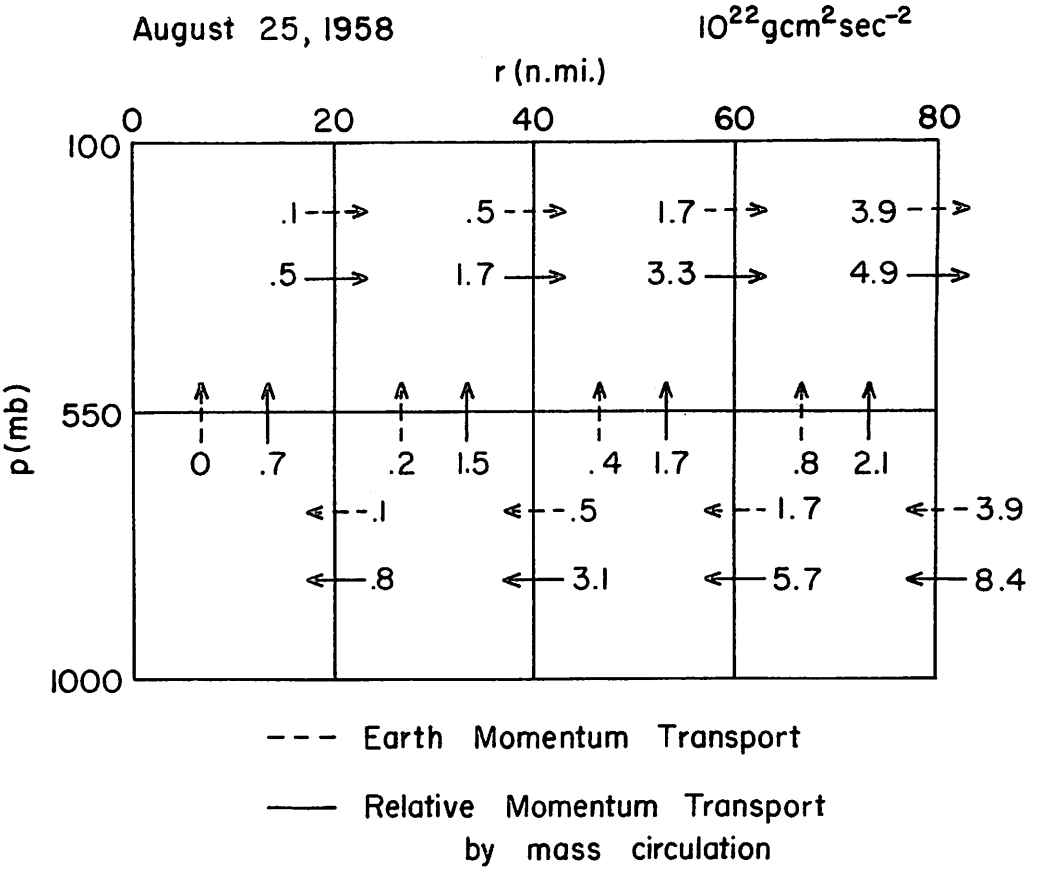

Figure 16. - Transport of absolute angular momentum by mass circulation on August 25.

Table 10. - Coefficient of horizontal turbulent exchange (μ_r) Unit: 10^6 g.cm.$^{-1}$ sec.$^{-1}$

	Radial interval (n.mi.)			
	0-40		40-80	
Aug. 25	0.7		1.5	
	0-20	20-40	40-60	60-80
Aug. 27	7.4	6.6	1.7	0.9

Values in table 10 superficially lie within the acceptable order of magnitude range; they are also time and space dependent. On August 25 a uniform value of 1 unit is suggested within the limits of accuracy of the data. The same value applies on August 27 outside the 60-mi. radius. In the interior, however, a strong rise in turbulence is indicated.

As a check whether the order of magnitude in table 10 is acceptable, the momentum budget will be computed in the next section. It will be shown there, what is not obvious from the energy calculations, namely that the large values of μ_r imply unreasonably large amounts of momentum transport outward, much

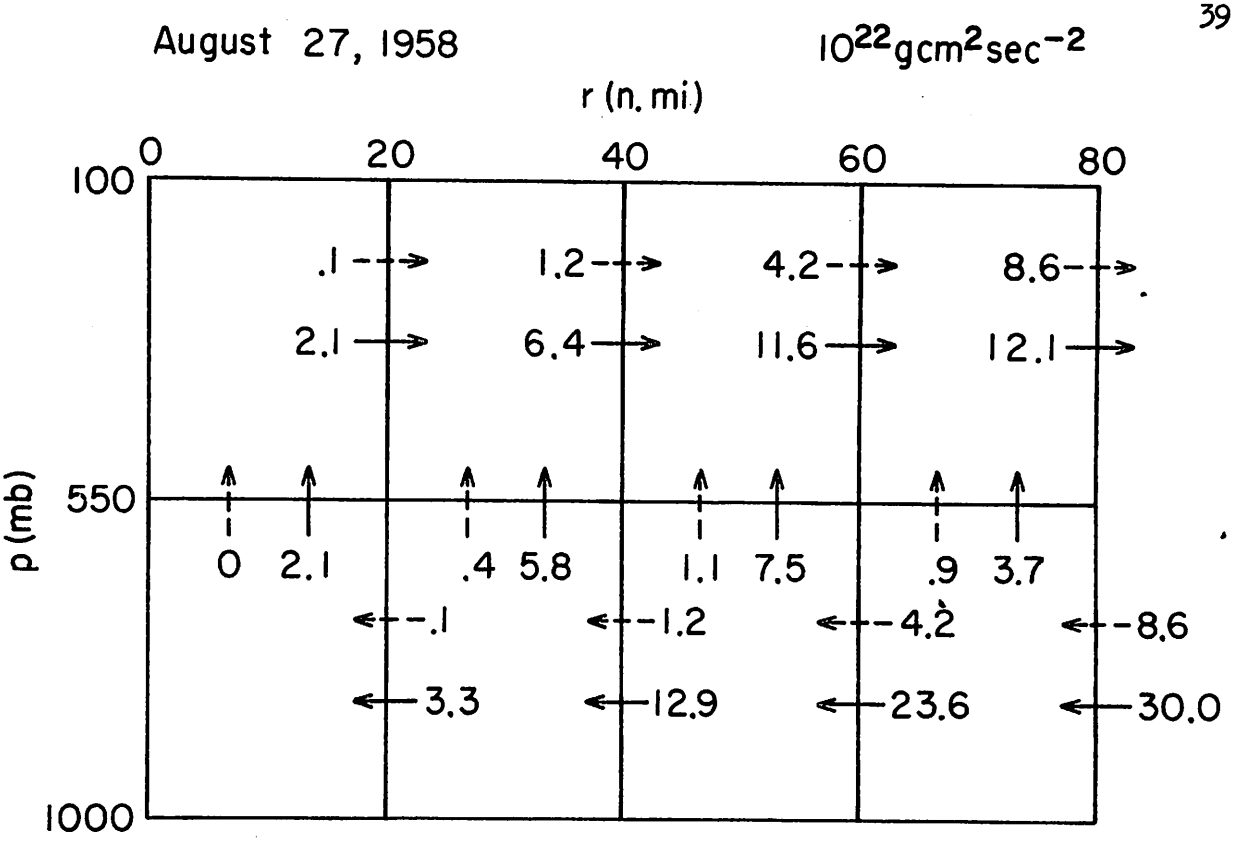

Figure 17. - Transport of absolute angular momentum by mass circulation on August 27.

more than can be ascribed to the range of error in our calculations. It follows that the high coefficients of table 10 must be rejected and that in all likelihood internal dissipation of kinetic energy takes place by means of vertical turbulence.

One other aspect of the large internal dissipation should be brought out. If all energy dissipated by this mechanism were to go into sensible heat,

$$IF = c_p \frac{dT}{dt} M, \qquad (21)$$

where dT/dt is the mean temperature change of the mass M due to internal friction. Of course, IF may go over into other energy forms. But, assuming equation (21) to hold, we obtain temperature changes as shown in table 11. In the core, values are very large indeed. Of course, individual air particles will seldom, if ever, remain there for a whole day. But if they merely stay inside the 40-mi. radius for 12 hours, net warming of 1° - 2°C. can result. This is the order of magnitude of the radiational cold source; hence in terms of source and sink computations the effect is by no means negligible.

Table 11. - Substantial temperature change (°C. day^{-1}) due to IF

	Radial Interval (n.mi.)			
	0-20	20-40	40-60	60-80
Aug. 27	4.0	1.8	0.8	0.1

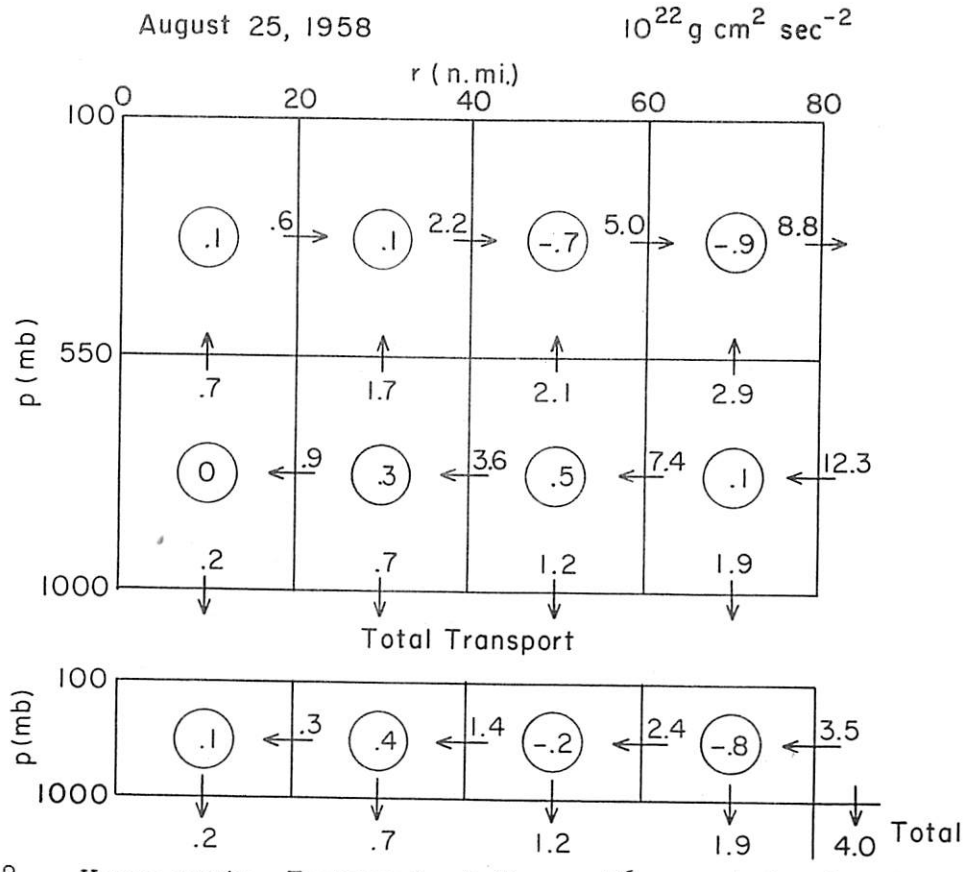

Figure 18. - Upper part: Transport of figure 16 repeated, also transfer to ocean and residuals in circles on August 25. Lower part: total lateral momentum transport, transfer to ocean and residuals.

8. THE BUDGET OF ABSOLUTE ANGULAR MOMENTUM

The momentum balance will be taken up in stationary coordinates, and several terms will be omitted which arise when the origin of the coordinate system is referred to a moving frame. Since storm propagation was very slow, this is considered to be a permissible simplification of a computational system which otherwise would be quite complicated. The momentum equation, including vertical and lateral stress terms, then is given by

$$\rho \frac{d\Omega}{dt} = \rho \frac{d}{dt}\left(ur + \frac{fr^2}{r}\right) = -\frac{\partial p}{\partial \theta} + \mu_z r \frac{\partial \tau_{\theta z}}{\partial z} + \mu_r r \frac{\partial \tau_{\theta r}}{\partial r}, \qquad (22)$$

where a constant Coriolis parameter f has been used. With the continuity equation $\rho \frac{d\Omega}{dt} = \frac{\partial \rho \Omega}{\partial t} + \nabla \cdot \rho \Omega \mathbf{V}$. Neglecting $\frac{\partial \rho \Omega}{\partial t}$ and integrating over the volume $\mathcal{A}$

$$\int_\sigma \rho \Omega c_n d\sigma = -\int r \tau_{\theta 0} dA + \mu_r \int r \frac{\partial \zeta_\theta}{\partial r} d\alpha. \qquad (23)$$

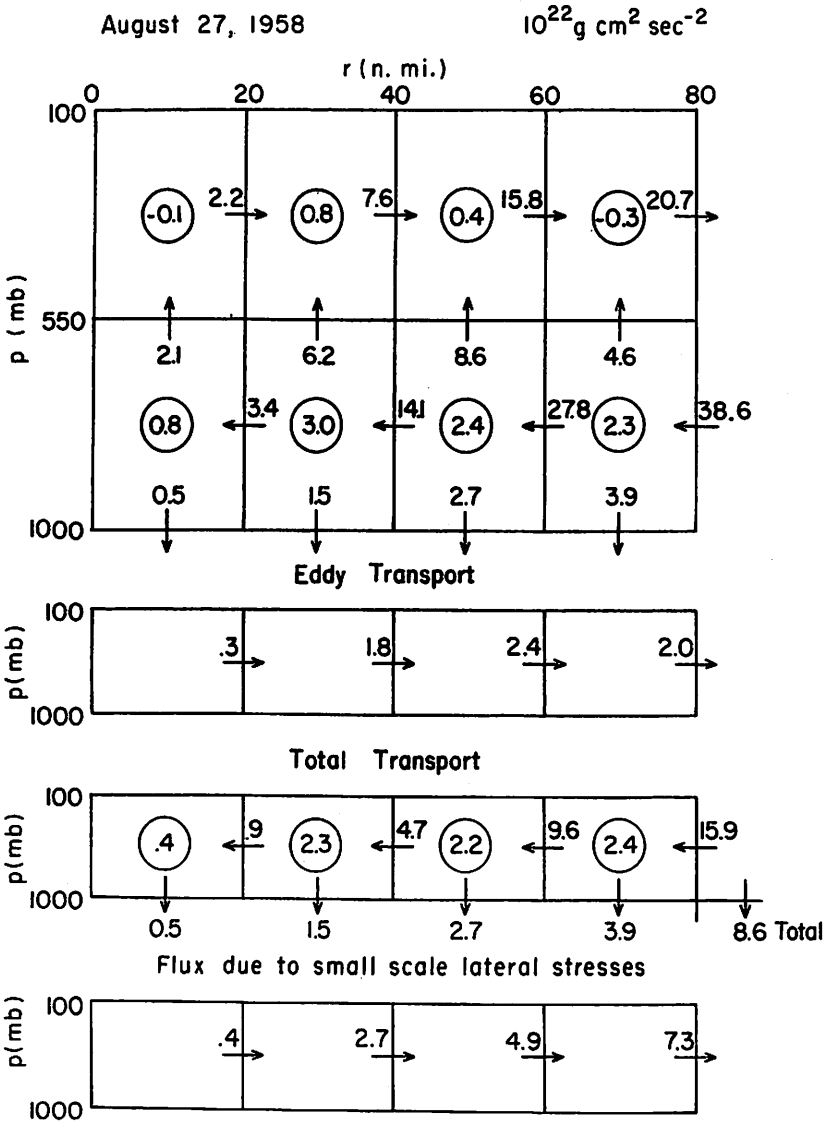

Figure 19. - Same as figure 18 for August 27, with intermediate line for eddy momentum flux. Residual to be exported by small-scale eddy stresses shown in line at bottom.

Here the advective term has been transformed to a surface integral over the bounding surface, and it has been assumed that the stress vanishes at the top of the storm. If the surface integral in equation (23) is evaluated between two radii and from the ground to the top of the system,

$$\int_\sigma \rho \Omega c_n d\sigma = \iint \Omega v r d\theta \frac{dp}{g} \Big]_{r_2} - \iint \Omega v r d\theta \frac{dp}{g} \Big]_{r_1}. \qquad (24)$$

Contributions to advection arise (cf. Palmén and Riehl [22]) from the transport of relative and of earth's angular momentum by the mass circulation, and from the correlations of u with v and w. Figures 16 and 17 show the fluxes due to the mass circulation integrated over the layers of inflow and outflow.

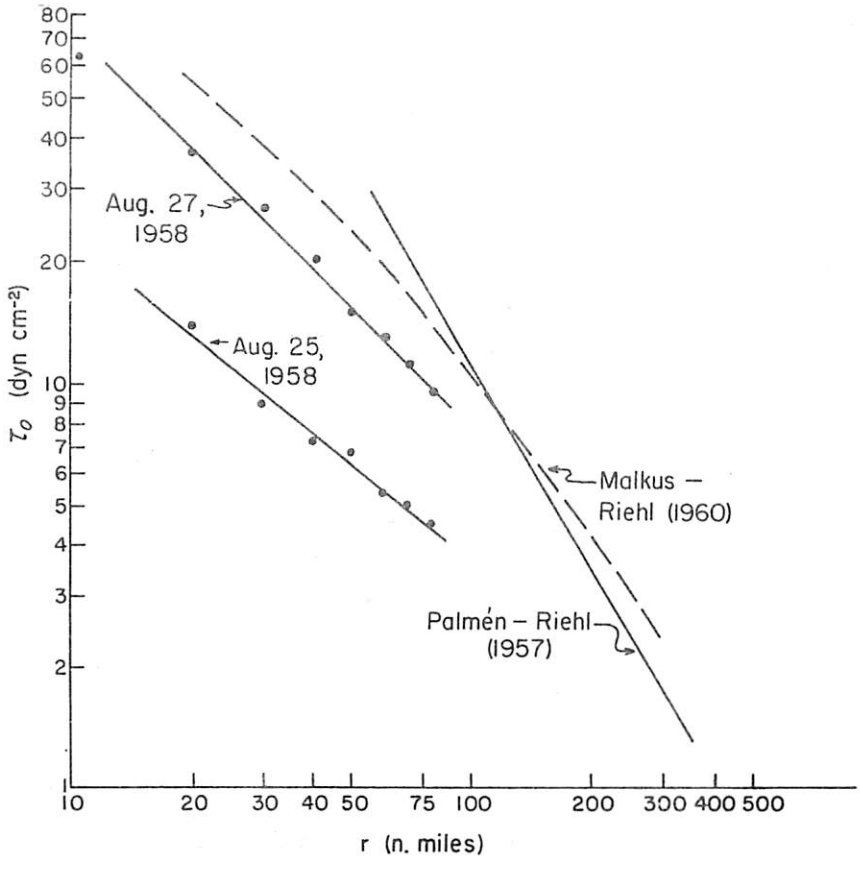

Figure 20. - Distribution of surface stress in Daisy and comparison with previous calculations.

The transport of the earth's angular momentum makes no contribution to the net balance. It is of importance, however, for determination of the vertical fluxes. Figures 18 and 19 contain the same fluxes, together with the residuals to be balanced and, in the lower portion, the net balance for the whole troposphere on each day. As in the kinetic energy budget, the correlation of u' and v' contributed very little on August 25 and acted to transfer momentum outward on August 27. The momentum flux to the surface was calculated from

$$\int \gamma \tau_{\theta 0} dA = \int c_D \rho_0 V_{\theta 0} V_0 \, dA, \qquad (25)$$

where on the 27th the 620-mb. wind distribution was used to represent the surface wind field as in the energy budget. Figure 20 shows the distribution of τ_0 which is very similar to that of $\tau_{\theta 0}$.

Transfer to the sea more than doubled between the two days; but it still was well below that computed by Palmén and Riehl [22] for the mean hurricane on the 27th. This is due to the fact that, as mentioned earlier, Daisy's winds were much weaker than those of the mean hurricane. On the 25th the inward transport of momentum by the mass circulation equalled the transport to the ocean within the limits of accuracy of the calculations. The eddy fluxes, as already mentioned, proved to be small and of uncertain sign, as in the case of the energy calculations. External forcing of the storm by eddy import

of absolute angular momentum into the inner region was NOT the mechanism that gave birth to Daisy.

The slight imbalance on the 25th could result from some underestimate of the inflow or overestimate of the transport to the ground. It could well be that outside the 40-mi. radius c_D was less than .0025 since winds decreased rapidly outward and were only 20-30 kt. beyond the 60-mi. radius. On the other hand, there is certainly nothing left over for lateral re-export by small-scale stresses. If $\mu_r = 1 \times 10^6$ g.cm.$^{-1}$sec.$^{-1}$ computed in Table 10 for August 25 is used in the lateral stress term of equation (23), an outward transport through the 80-mi. radius is computed which is about twice the total import by the mass circulation. It follows that the lateral exchange coefficient must have a magnitude of not more than 10^5 g.cm.$^{-1}$sec.$^{-1}$ on that day for momentum balance, and that therewith dissipation of kinetic energy also must have taken place mainly by means of vertical eddies.

On the 27th a small amount of momentum was exported by the $\overline{u'v'}$ correlation so that this type of stress, far from importing momentum, actually removed it from the core as also on most other occasions where calculations have been performed. After taking account of this transport about half of the imported momentum was given off to the ocean surface, and the balance on this day must be re-exported by small-scale lateral stresses. If the coefficients of table 10 are used for this purpose, the outward flux exceeds the total import by a very large amount, almost an order of magnitude. If a uniform coefficient of 1×10^6 g.cm.$^{-1}$sec.$^{-1}$ is taken, the export across the 80-mi. radius is 9.5 units. From the bottom of figure 19, the required export is 7.3 units. Hence this order of magnitude of the coefficient is satisfactory on the 27th. The lateral exchange still rises by an order of magnitude as the hurricane matured.

In conclusion of the energy and momentum sections the following may be summarized:

(1) The inward momentum and energy transport took place by means of the mass circulation.

(2) "Eddy" transports of angular momentum and energy were negligible or were directed outward.

(3) Transport of momentum to the ocean very nearly satisfied balance requirements on the 25th. There is no need to invoke lateral momentum export by small-scale stresses. Hence the internal dissipation of kinetic energy - equal to the ground dissipation in the core - must have taken place by means of vertical eddies. The lateral exchange coefficient μ_r has a magnitude of not more than 1×10^5 g.cm.$^{-1}$sec.$^{-1}$.

(4) On August 27 interaction with the ground did not satisfy momentum balance. At this well-developed stage it is necessary to postulate lateral

momentum export with coefficient of 1×10^{6} g.cm.$^{-1}$ sec.$^{-1}$, hence one order of magnitude larger than on August 25. Therefore this constraint upon the storm's growth becomes important. However, lateral coefficients computed from the momentum and energy budgets are not compatible if the assumption is made that all momentum transfer and all energy dissipation go by way of this process. One must postulate that the kinetic energy is dissipated by vertical turbulence. This requires a coefficient μ_z of 100 g. cm.$^{-1}$ sec.$^{-1}$; this is not considered excessive.

(5) Internal dissipation on the 27th became so strong as to be able to affect the heat budget. If the energy dissipated is converted to sensible heat, a source with magnitude of Q_s is obtained inside the 40-mi. radius.

(6) There are strong indications that the surface dissipation of kinetic energy is independent of distance from the center, and that this may be a general feature of hurricanes which explains the observed surface wind profile along the radius.

(7) The calculations have shown that both from momentum and energy viewpoints resistance against storm growth rose rapidly with intensification due to increasing importance of lateral and vertical turbulence. This is, however, no reason to suppose that this increase in the magnitude of the resistive effects relative to the generative terms is not present in each instance of storm development. Hence the calculations shed no light on the question why some hurricanes remain minimal while others rise to great intensity. It is probably that the peak intensity of each hurricane is controlled by external, not internal, factors.

9. TWO-DIMENSIONAL ANALYSIS AND CONCLUSIONS

The question may be asked what the results of this study portend with respect to understanding the hurricane engine, and with respect to future researches and observations. As case histories accumulate, one can of course proceed from the hundredth to the thousandth detail and demonstrate certain differences between individual storms. But is it worthwhile to do this? What can be said more generally about the mechanisms of hurricane maintenance from the present data? Is it necessary to treat a vortex, fully turbulent along all coordinates, and with turbulence also time dependent? How important is it that the air winds its way inward in rather tortuous selective channels which produce micro-patterns in the horizontal velocity field and that the bulk of the ascent appears concentrated in hot towers covering only a small fraction of the hurricane's area?

The Daisy data have in fact confirmed the importance of the hot tower mechanism and the concentration of the storm's heat release into 100-200 individual buoyant elements. If the details of the activity on these small scales are decisive for storm growth and maintenance, then the prospect for solving the large-scale hurricane problems and achieving predictive models recedes into the dim future. We shall conclude by offering the hope that the dynamic and thermal effects of these small scales of motion can be introduced or parameterized effectively in a relatively simple framework, without dwelling on their complex details which may differ from cases to case and from time to time.

The most favorable situation would exist if it can be shown that the significant features of the hurricane can be grasped with two-dimensional models. In this respect, a hopeful start was made by Malkus and Riehl [19]. The preceding Daisy calculations are promising along the same line in that lateral eddy transports of heat and moisture proved small, and especially in that the much-vaunted u'v' correlation was small with sign opposite to that postulated by its proponents; even the kinetic energy transport by the K'v' correlation on August 27 was small enough so that it could have been neglected within limits of all other calculations. Outside the core, the u'v' correlation appears to act in the same sense as in the core, at least to several hundred miles distant from a hurricane center (Riehl [24]).

Some of the interior mechanisms whose magnitudes are significant and which have been assessed here, such as internal and boundary friction along vertical and lateral axes may be expected to develop during any successful storm and hence should most probably be treated as necessary but dependent features, as should the local heat source, provided of course that the hurricane does not move to an area of much lower ocean temperatures or over land.

Two constraints upon hurricane development have been emphasized: ventilation and internal energy dissipation. Of these constraints, ventilation is a function of external parameters as far as one can see now. The question of what governs the vertical distribution of inflow stands out as one of the most important unresolved problems raised for future investigation.

Internal energy dissipation, according to our hypothesis, results from selective ascent of air in narrow channels. An indicated above, air moves from bottom to top of the troposphere in these channels in about 30 minutes; hence the tendency toward conservation of momentum and energy during such ascent is high, and a large decrease of kinetic energy must occur when mixing finally does take place in the upper troposphere.

On the whole, simple models such as developed by Palmén and Riehl [22] and by Malkus and Riehl [19] have been supported by the present calculations. For guidance in development of complete two-dimensional models and quantitative prediction of hurricanes it appears appropriate, therefore, to present in closing a few illustrations of Daisy as this storm appears in two-dimensional form. First, the mass flow of figures 5 and 6 may be represented in the form of Stokes' stream functions (figs. 21-22). For this calculation the same vertical and radial intervals were used as in figures 5 and 6. As already emphasized, the main feature in which the mass flow deviates from earlier models is the high level of non-divergence which results in importation of air with lower heat content than that of the surface layer. On August 25 the streamlines, which are also trajectories of the steady-state motion, and the lines of equal Q are fairly parallel, except in the inner core (fig. 23). On the 27th (fig. 24), the trajectories cross more strongly toward higher Q above the level of non-divergence, indicating increased effects of the oceanic heat source and transfer by rising undilute cumulonimbi and the mass they shed. Thus, in two-dimensional representation, the selective vertical motion in hot towers can be replaced by a mean vertical motion spread over the whole area, but only if $\tilde{Q}$ is replaced by $\overline{Q}$ for the vertical redistribution of heat.

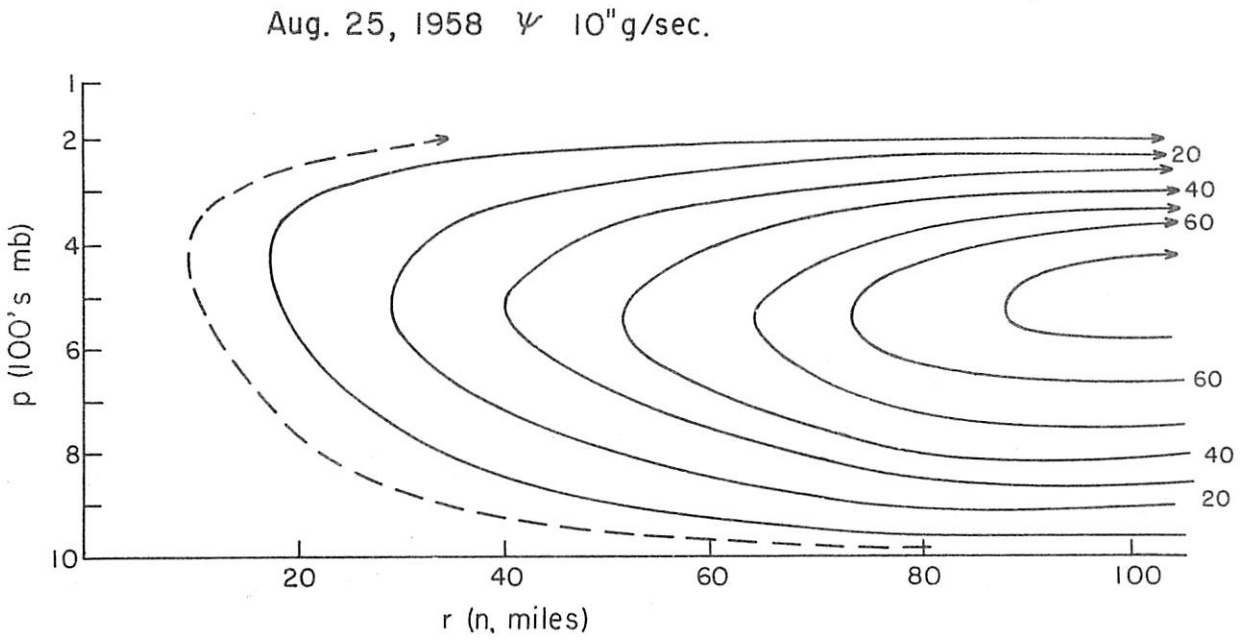

Figure 21. - Stokes stream function (units 10^{11} g.sec.$^{-1}$) for August 25.

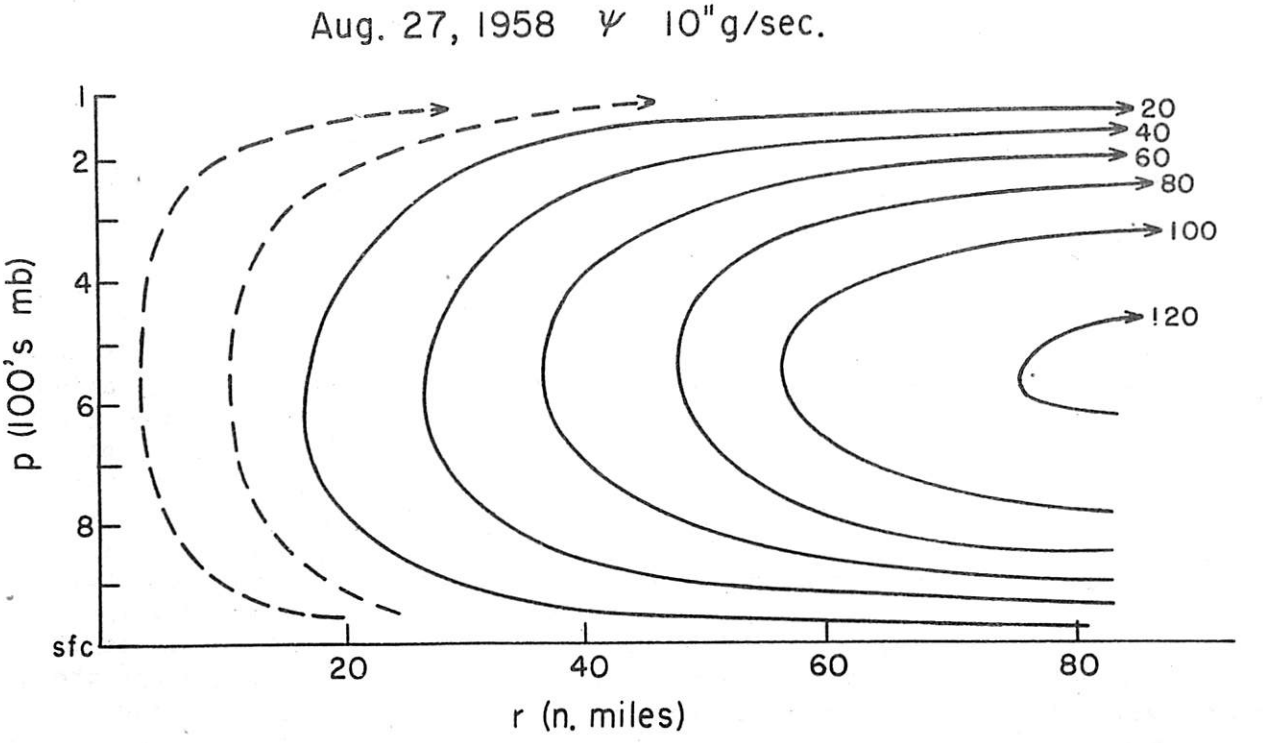

Figure 22. - Stokes stream function (units 10^{11} g. sec.$^{-1}$) for August 27.

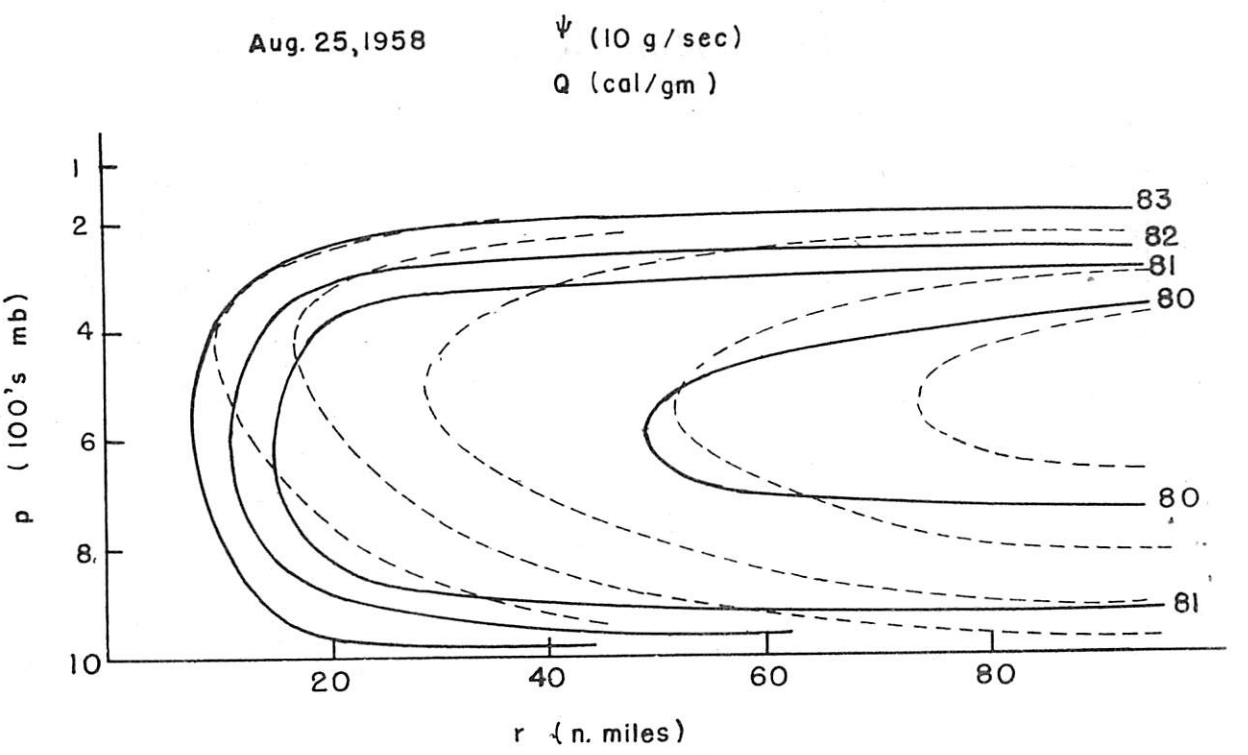

Figure 23. - Stokes stream function (dashed) and lines of constant heat content (solid) for August 25.

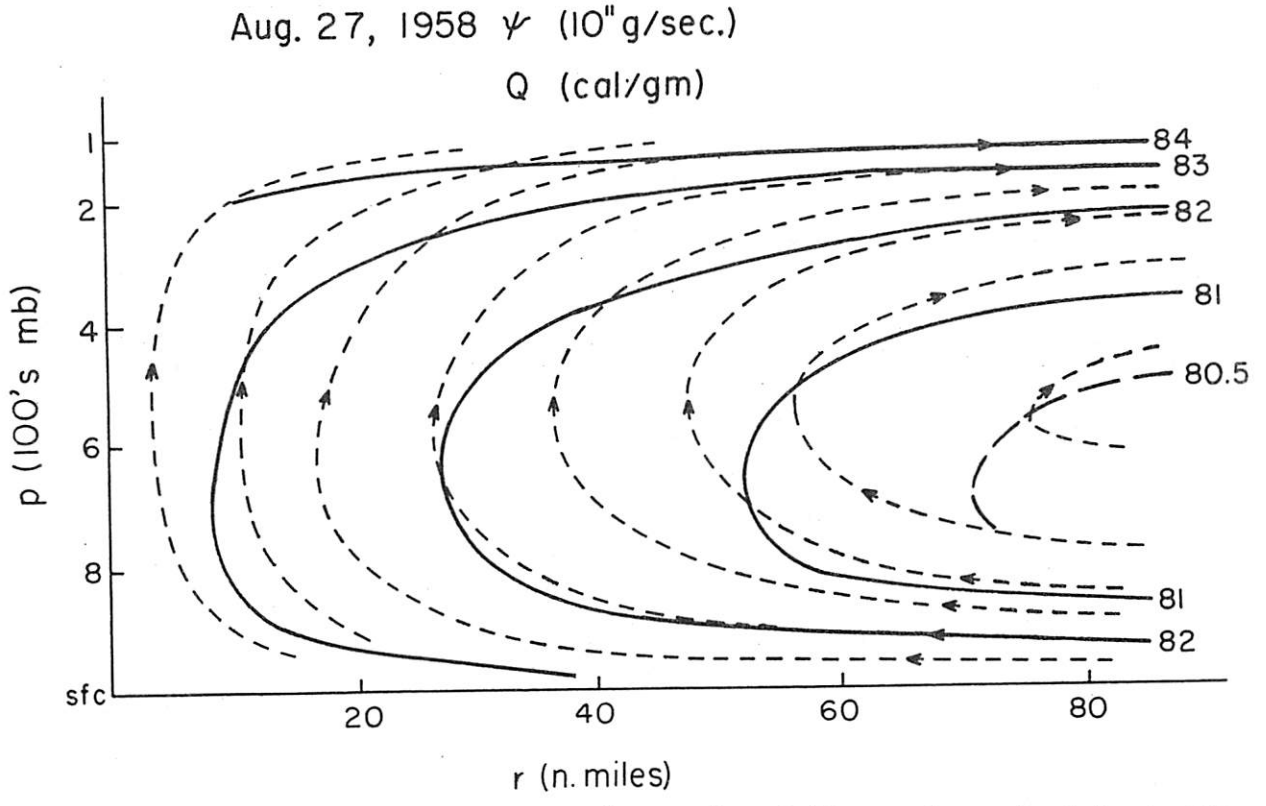

Figure 24. - Stokes stream function (dashed) and lines of constant heat content (solid) for August 27.

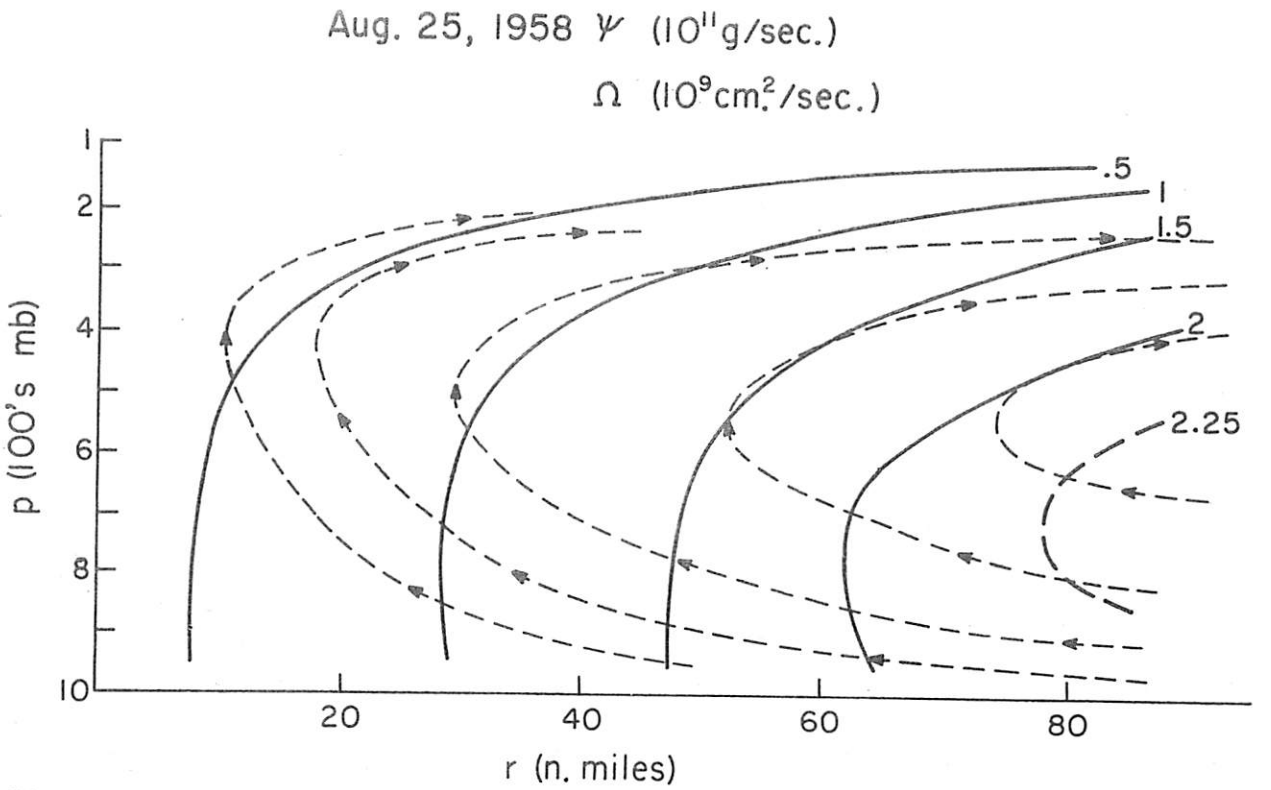

Figure 25. - Stokes stream function (dashed) and lines of constant absolute angular momentum (solid) for August 25.

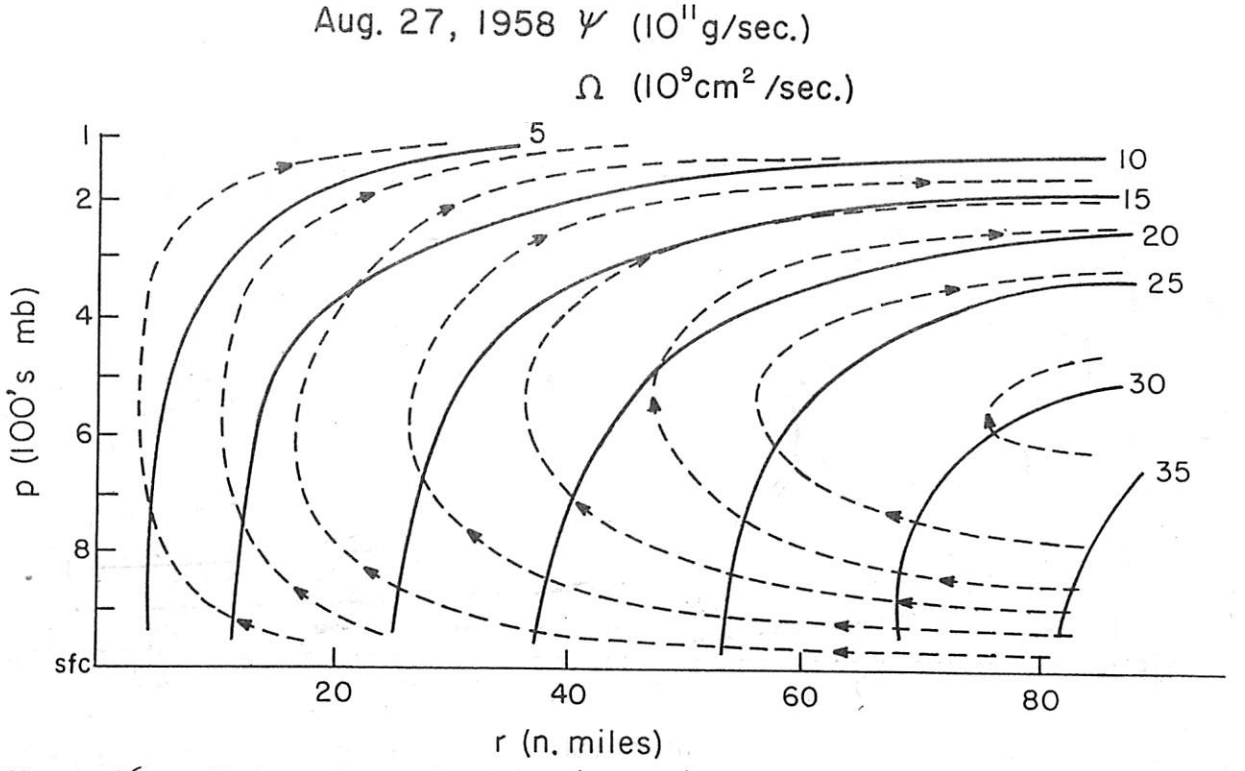

Figure 26. - Stokes stream function (dashed) and lines of constant absolute angular momentum (solid) for August 27.

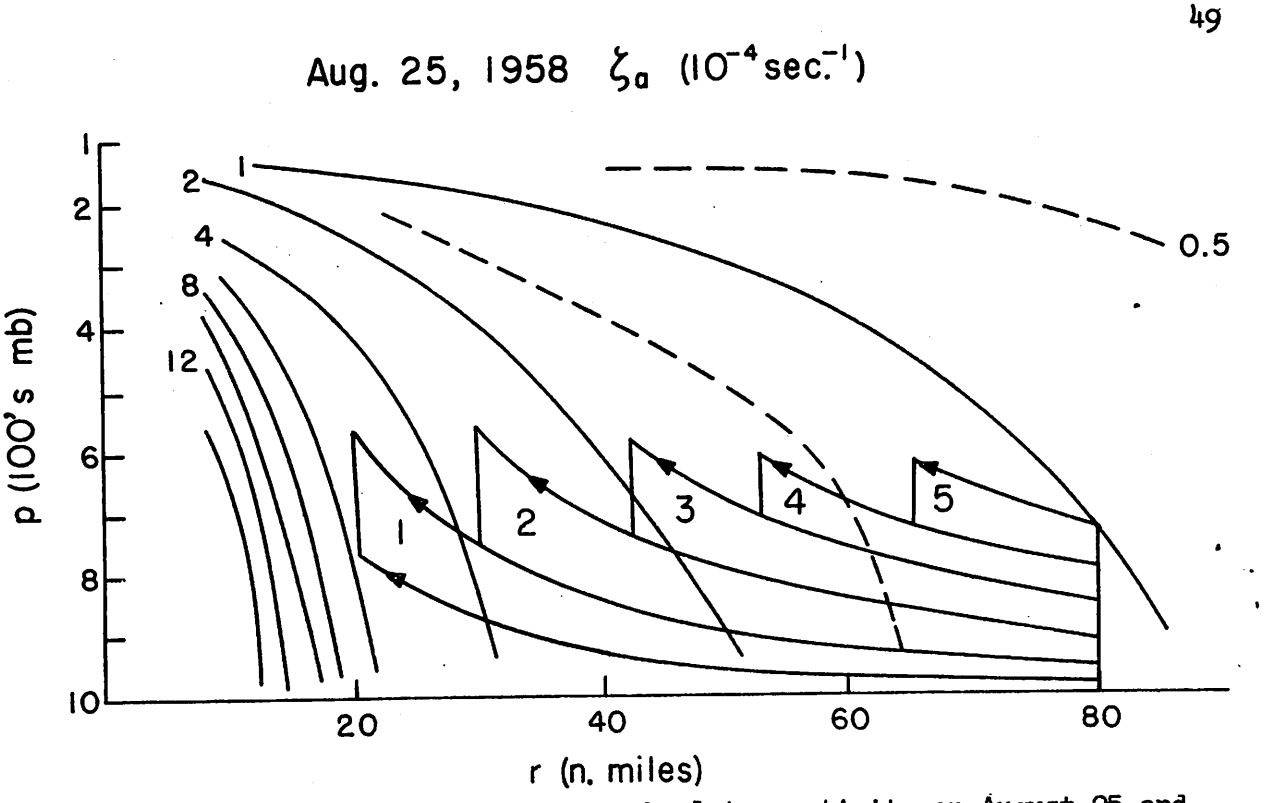

Figure 27. - Vertical cross section of absolute vorticity on August 25 and selected streamtubes from figure 21.

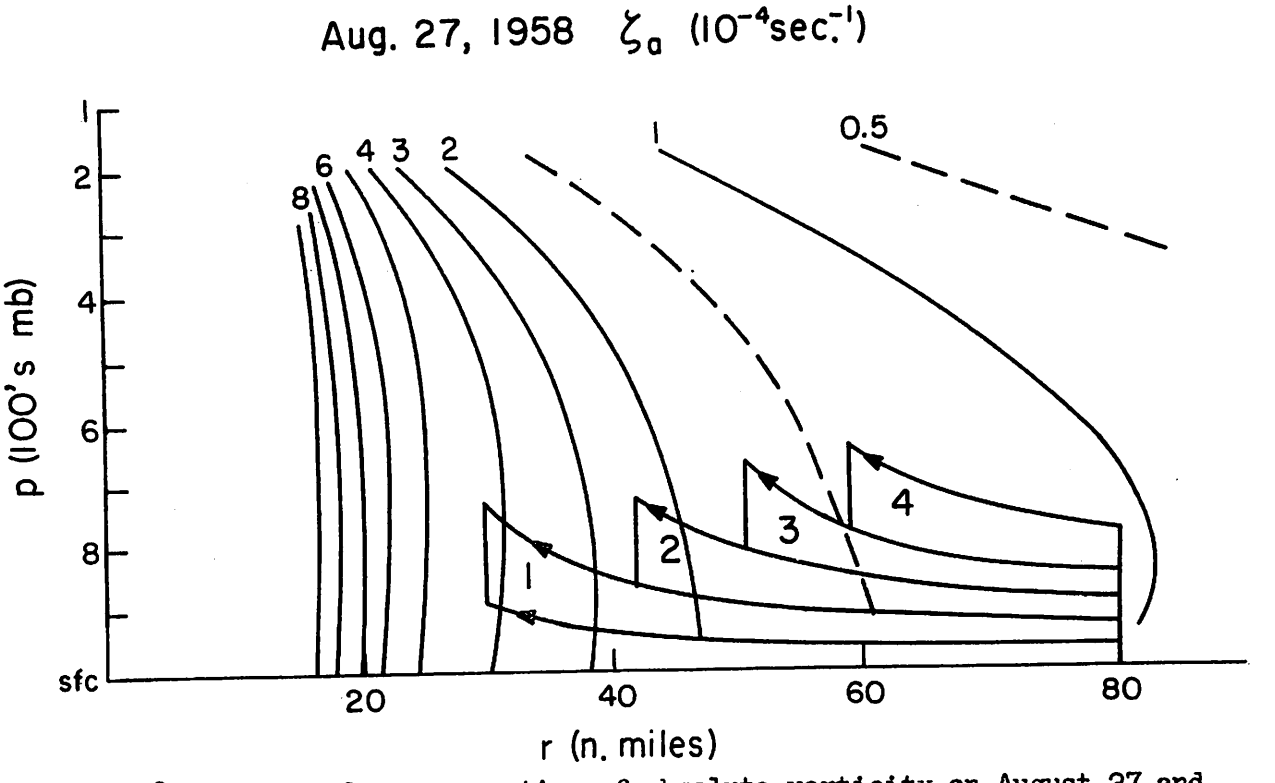

Figure 28. - Vertical cross section of absolute vorticity on August 27 and selected streamtubes from figure 22.

The streamlines also cross toward lower absolute angular momentum up to the level of non-divergence on the 25th (fig. 25), while higher up the momentum is roughly constant along these lines. This extension of the "friction layer" to the whole inflow layer must be accepted as realistic. It indicates the depth to which the flow is essentially controlled by transfer processes at the ocean surface and may be thought to correspond to the depth of the cloud layer in the trades (Riehl and Malkus [28]). On August 27 (fig. 26) the streamlines cross toward lower momentum at least up to 300 mb., and this might be taken to reflect the rising importance of lateral shearing stresses on that day. In the outflow layer the momentum again is as constant as drawing within observational limits permits.

We wish finally to investigate further whether the mean streamfunction representation of figures 21 and 22 also is promising from the vorticity standpoint. While undoubtedly there are frictional influences on the vorticity field, it may still be presumed that the major configuration of the vorticity field is linked to the distribution of convergence and divergence so that, in the first approximation, the theorem of conservation of potential vorticity may hold. If so,

$$\frac{\xi_{a_2}}{\xi_{a_1}} = \frac{\Delta p_2}{\Delta p_1}, \qquad (26)$$

where ξ_a is the absolute vorticity, Δp the pressure-depth of the column considered, and the integration is carried out between the radii r_2 and r_1. Figures 27-28 contain the absolute vorticity cross sections, which are rather similar. Equation (25) was tested for five streamtubes of the inflow layer on the 25th and for four tubes on the 27th. No calculations were performed in the outflow region, but one can see qualitatively by comparison with figures 21-22 that decreasing ξ_a and Δp coincide. Table 12 gives the results for the inflow layer, where it must be noted that only rough answers can be expected in view of the uncertainties in drawing the streamtubes, especially at the 80-mi. radius which was taken as r_1.

Agreement is satisfactory, especially along the mean trajectories which have the largest pressure changes; altogether percentages decrease together for ξ_{a_2}/ξ_{a_1} and $\Delta p_2/\Delta p_1$. Hence, from the dynamical viewpoint, it will be quite legitimate to treat the streamfunction field as representing the synoptic scale motion in Daisy. This outcome is particularly gratifying, as it is just the vorticity aspect of the hurricane which might have been affected strongly by the hot tower ascents which, after all, cross the mean streamtubes everywhere except perhaps in the eye wall.*

Given conservation of potential vorticity in a steady two-dimensional field, the transport of absolute vorticity is constant after integration over, say, the inflow layer. This property of constant vorticity transport was used

*It should be noted again that all calculations of this paper refer only to the hurricane outside the eye wall.

Table 12. - Test of conservation of potential vorticity

	Streamtube				
	1	2	3	4	5
August 25					
ξ_{a_2}/ξ_{a_1}	4.5	3.2	1.8	1.5	1.3
$\Delta p_2/\Delta p_1$	4.5	3.6	2.5	1.6	1.5
August 27					
ξ_{a_2}/ξ_{a_1}	4.1	2.3	1.5	1.4	-
$\Delta p_2/\Delta p_1$	4.5	3.5	2.8	1.8	-

by Riehl and Fultz [27] to compute the velocity profile in a three-wave dishpan experiment and by Krishnamurti [14] to determine the velocity field of the subtropical jet stream. The calculation appears promising also for the hurricane since the vorticity increases as the mass flow decreases inward. Then

$$\xi_a \, Mr = \text{const}\ (r). \tag{27}$$

Table 13 contains the result. Within reasonable limits the vorticity flux is constant.

In conclusion, it appears hopeful to attempt two-dimensional models of the hurricane core, provided the vital convective-scale processes are adequately parameterized and entered in the thermal budgets where their transports and releases are vital in the basic machinery. It appears likely that scales of motion intermediate between convection and the hurricane itself, such as lateral eddy transports, are not essential in the core; thus a "separation of scales of motion" may provide a framework of future useful attack upon this problem, as it has for other thermally-driven circulations in the Tropics (Malkus [16]).

Table 13. - Transport of absolute vorticity in inflow layer, unit: 10^8 g.sec.$^{-2}$

	Radius (n.mi.)			
	20	40	60	80
August 25	6.7	7.0	6.0	6.0
August 27	14.2	14.6	14.0	13.0

ACKNOWLEDGMENT

This work could not have been executed without the remarkable achievement of the National Hurricane Research Project in obtaining the three days of flight records in Daisy, their care in reducing these, and their generosity and constant effort in providing them to us, supplemented by their experienced assistance at every phase. We are especially grateful to the directors of this program, R. H. Simpson, R. C. Gentry, and H. F. Hawkins.

The research was supported by the Office of Naval Research and the United States Weather Bureau.

REFERENCES

1. M. Ausman, "Some Computations of the Inflow Angle in Hurricanes Near the Ocean Surface," Dept. of Meteorology, University of Chicago, Report under Contract No. N6 ori-02036 to Office of Naval Research, 1959. (Unpublished)
2. J. Colón et al., "Hurricane Daisy, 1958," 1961. (To be issued in NHRP Report series.
3. E. L. Deacon, P. A. Sheppard, and E. K. Webb, "Wind Profiles Over the Sea and the Drag at the Sea Surface," Australian Journal of Physics, vol. 9, No. 4, Dec. 1956, pp. 511-514.
4. A. Defant, "Die Zirkulation der Atmosphäre in den Gemassigten Breiten der Erde," Geografiska Annaler, Bd. 3, 1921, p. 209.
5. M. Gangopadhyaya and H. Riehl, "Exchange of Heat, Moisture, and Momentum Between Huuricane Ella (1958) and Its Environment," Quarterly Journal of the Royal Meteorological Society, vol. 85, No. 365, July 1959, pp. 278-286.
6. M. Garstang, "Some Meteorological Aspects of the Low-Latitude Tropical Western Atlantic," Woods Hole Oceanographic Institution, 1958,97 pp., (unpublished).
7. W. M. Gray, "On the Balance of Forces and Radial Accelerations in Hurricanes," Atmospheric Sciences Research, Report No. 1, Colorado State University, 1961.
8. G. Grimminger, "The Intensity of Lateral Mixing in the Atmosphere As Determined from Isentropic Charts," Transactions, American Geophysical Union, vol. 19, 1938, p. 163.
9. H. V. Groening, "Wind and Pressure Fields in the Stratosphere Over the West Indies in August 1958," National Hurricane Research Project Report No. 35, 1960, pp.
10. D. T. Hilleary and F. E. Christensen, "Instrumentation of National Hurricane Research Project Aircraft," National Hurricane Research Project Report No. 11, 1956, 71 pp.
11. L. A. Hughes, "On the Low-Level Wind Structure of Tropical Storms," Journal of Meteorology, vol. 9, No. 6, Dec. 1952, pp. 422-428.
12. C. L. Jordan, D. A. Hurt, Jr., and C. A. Lowry, "On the Structure of Hurricane Daisy on 27 August 1958," Journal of Meteorology, vol. 17, No. 3, June 1960, pp. 337-348.
13. E. S. Jordan, "An Observational Study of the Upper Wind-Circulation Around Tropical Storms," Journal of Meteorology, vol. 9, No. 5, Oct. 1952, pp. 340-346.

14. T. N. Krishnamurti, "The Subtropical Jet Stream of Winter," Journal of Meteorology (to be published).
15. D. W. Krueger, "A Relation Between the Mass Circulation Through Hurricanes and Their Intensity," Bulletin of the American Meteorological Society, vol. 40, No. 4, Apr. 1959, pp. 182-190.
16. J. S. Malkus, "On the Maintenance of the Trade Winds," Tellus, vol. 8, 1956, pp. 335-350.
17. J. S. Malkus, "On the Thermal Structure of the Hurricane Core." Proceedings, Technical Conference on Hurricanes, Miami, Fla., Nov. 1958, American Meteorological Society, 1958, D3, pp. 1-2.
18. J. S. Malkus, "Recent Developments in the Study of Penetrative Convection and an Application to Hurricane Cumulonimbus Towers," Proceedings, First Conference on Cumulus Convection, Wentworth, N. H., 1959, 1960, pp. 65-84.
19. J. S. Malkus and H. Riehl, "On the Dynamics and Energy Transformation in Steady-State Hurricanes," Tellus, vol. 12, No. 1, Feb. 1960, pp. 1-20.
20. J. S. Malkus, C. Ronne, and M. Chaffee, "Cloud Patterns in Hurricane Daisy, 1958," Woods Hole Oceanographic Institution, Technical Report No. 8 on grant NSF 7368, Jan. 1960.
21. B. I. Miller, "The Three-Dimensional Wind Structure Around a Tropical Cyclone," National Hurricane Research Project Report, No. 15, 1957.
22. E. Palmén and H. Riehl, "Budget of Angular Momentum and Energy in Tropical Cyclones," Journal of Meteorology, vol. 14, No. 2, Apr. 1957, pp. 150-159.
23. C. H. B. Priestley, Turbulent Transfer in the Lower Atmosphere, The University of Chicago Press, Chicago, Ill., 1959, 130 pp.
24. H. Riehl, "On the Mechanisms of Angular Momentum Transport in Hurricanes," Journal of Meteorology, vol. 18, No. 1, Feb. 1961, pp. 113-115.
25. H. Riehl, Tropical Meteorology, McGraw-Hill Book Co., Inc., New York, 1954, 394 pp.
26. H. Riehl et al., "The Northeast Trade of the Pacific Ocean," Quarterly Journal of the Royal Meteorological Society, vol. 77, 1951, pp. 598-626.
27. H. Riehl and D. Fultz, "The General Circulation in a Steady Rotating Dishpan Experiment," Quarterly Journal of the Royal Meteorological Society, vol. 84, No. 362, Oct. 1958, pp. 389-417.
28. H. Riehl and J. S. Malkus, "On the Heat Balance and Maintenance of Circulation in the Trades," Quarterly Journal of the Royal Meteorological Society, vol. 83, No. 355, Jan. 1957, pp. 21-29.
29. H. Riehl and J. S. Malkus, "On the Heat Balance in the Equatorial Trough Zone," Geophysica, vol. 6, No. 3-4 Meteorology, 1959, pp. 503-538.
30. R. H. Simpson and H. Riehl, "Mid-Tropospheric Ventilation as a Constraint on Hurricane Development and Maintenance," Proceedings, Technical Conference on Hurricanes, Miami, Fla., Nov. 1958, American Meteorological Society, 1958, D4, pp. 1-10.

APPENDIX

QUANTITIES FOR LATERAL FLUX CALCULATIONS

1. Temperature T (°C.)

August 25					
Pressure	Radius (n.mi.)				
(100's mb.)	20	40	60	80	100
2-1.5	-58.1	-58.9	-59.0	-59.0	-59.0
3-2	-38.0	-39.0	-39.3	-39.5	-39.5
4-3	-21.7	-22.7	-23.0	-23.1	-23.1
5-4	- 9.9	-11.1	-11.5	-11.9	-11.9
6-5	- 1.1	- 2.3	- 2.5	- 2.8	- 2.8
7-6	5.9	5.1	4.9	4.9	4.9
8-7	11.7	11.1	11.0	11.0	11.0
9-8	16.8	16.3	16.2	16.1	16.1
10-9	21.7	21.2	21.1	21.0	21.0

August 27					
Pressure	Radius (n.mi.)				
(100's mb.)	15	20	40	60	80
1.5-1	-69.4	-69.8	-71.1	-72.2	-72.7
2-1.5	-52.6	-53.2	-55.7	-57.5	-59.0
3-2	-33.8	-34.6	-37.3	-38.4	-39.8
4-3	-16.5	-17.4	-19.9	-21.1	-22.5
5-4	- 4.9	- 5.7	- 8.0	- 9.3	-10.5
6-5	3.5	2.7	0.8	- 0.6	- 1.6
7-6	9.9	9.0	7.6	6.4	5.6
8-7	15.1	14.6	13.4	12.3	11.4
9-8	19.8	19.4	18.3	17.3	16.6
sfc-9	24.0	23.7	23.3	22.9	22.6

2. Specific Humidity $\bar{q}$ ($g.kg.^{-1}$)

August 25					
Pressure (100's mb.)	Radius (n.mi.) 20	40	60	80	100
2-1.5	-	-	-	-	-
3-2	0.3	0.2	0.1	-	-
4-3	1.5	1.2	0.8	0.6	0.3
5-4	3.0	2.8	2.3	2.0	1.7
6-5	5.8	5.2	5.0	4.5	4.2
7-6	8.2	7.7	7.3	7.1	6.8
8-7	11.0	10.2	10.1	10.0	9.9
9-8	13.6	12.9	12.6	12.4	12.3
10-9	17.7	17.0	16.5	16.2	16.0
Total precip. moisture (g)	6.1	5.7	5.5	5.3	5.1

August 27					
Pressure (100's mb.)	Radius (n.mi.) 15	20	40	60	80
1.5-1	-	-	-	-	-
2-1.5	-	-	-	-	-
3-2	1.1	1.0	0.8	0.6	0.5
4-3	3.1	2.7	2.2	2.0	1.8
5-4	5.7	5.2	4.2	3.9	3.7
6-5	8.6	7.7	6.8	6.1	5.7
7-6	11.4	10.3	9.5	8.5	8.0
8-7	14.0	12.8	12.0	11.0	10.4
9-8	16.5	15.3	14.4	13.5	13.0
sfc-9	19.7	18.3	17.4	17.1	16.7
Total precip. moisture (g)	7.4	7.0	6.6	6.3	6.0

3. gD^* (10^6 cm.^{2} sec.$^{-2}$) D^* = deviation from mean tropical atmosphere

August 25							August 27						
Pressure (100's mb.)	Radius (n.mi.) 20	40	60	80	100	Height of mean tropical atmosphere (10's m.)	Pressure (100's mb.)	Radius (n.mi.) 15	20	40	60	80	Height of mean tropical atmosphere (10's m.)
2-1.5	6	7	5	3	2	1329	1.5-1	3	4	5	6	8	1536
3-2	4	3	2	2	2	1103	2-1.5	-19	-15	-14	-10	-6	1329
4-3	-3	1	0	1	1	862	3-2	-23	-19	-16	-14	-10	1103
5-4	-5	-1	-1	0	1	672	4-3	-28	-16	-13	- 9	- 7	862
6-5	-6	-3	-2	-1	1	515	5-4	-34	-18	-16	-12	- 9	672
7-6	-8	-4	-3	-1	0	380	6-5	-42	-21	-17	-13	-11	515
8-7	-9	-5	-3	-1	0	261	7-6	-43	-22	-16	-12	-11	380
9-8	-9	-6	-4	-1	-1	155	8-7	-44	-23	-16	-12	-11	261
10-9	-9	-6	-4	-2	-1	58	9-8	-46	-27	-19	-15	-11	155
							sfc-9	-46	-27	-19	-15	-11	76-58

4. $c_p \overline{T}$ (cal. gm.$^{-1}$)

August 25					
Pressure	Radius (n.mi.)				
(100's mb.)	20	40	60	80	100
2-1.5	51.4	51.2	51.2	51.2	51.2
3-2	56.2	55.9	55.9	55.8	55.8
4-3	60.1	59.8	59.8	59.7	59.7
5-4	62.9	62.6	62.5	62.4	62.4
6-5	65.0	64.7	64.7	64.6	64.6
7-6	66.7	66.5	66.4	66.4	66.4
8-7	68.0	67.9	67.9	67.9	67.9
9-8	69.3	69.1	69.1	69.1	69.1
10-9	70.4	70.3	70.3	70.3	70.3

August 27					
Pressure	Radius (n.mi.)				
(100's mb.)	15	20	40	60	80
1.5-1	48.9	48.7	48.4	48.2	48.1
2-1.5	52.9	52.8	52.2	51.8	51.4
3-2	57.4	57.2	56.6	56.4	56.0
4-3	61.6	61.3	60.7	60.4	60.1
5-4	64.4	64.1	63.6	63.3	63.0
6-5	66.4	66.2	65.7	65.4	65.1
7-6	68.0	67.8	67.2	67.1	66.9
8-7	69.1	69.0	68.7	68.5	68.2
9-8	70.3	70.2	69.9	69.7	69.5
sfc-9	71.3	71.2	71.1	71.1	71.0

5. $g\bar{z}$ (cal. $g.^{-1}$)

August 25					
Pressure	Radius (n.mi.)				
(100's mb.)	20	40	60	80	100
2-1.5	32.0	32.1	32.0	32.0	32.0
3-2	26.6	26.5	26.5	26.5	26.5
4-3	20.1	20.1	20.1	20.1	20.1
5-4	16.0	16.1	16.1	16.1	16.2
6-5	12.2	12.3	12.3	12.3	12.3
7-6	8.9	9.0	9.0	9.1	9.1
8-7	6.0	6.1	6.2	6.2	6.3
9-8	3.5	3.6	3.6	3.7	3.7
10-9	1.2	1.3	1.3	1.4	1.4

August 27					
Pressure	Radius (n.mi.)				
(100's mb.)	15	20	40	60	80
1.5-1	36.2	36.2	36.2	36.3	36.3
2-1.5	30.8	30.9	30.9	31.0	31.1
3-2	25.4	25.5	25.5	25.6	25.7
4-3	19.6	19.9	20.0	20.0	20.1
5-4	15.0	15.4	15.5	15.5	15.6
6-5	11.2	11.7	11.8	11.8	11.9
7-6	7.9	8.4	8.5	8.6	8.7
8-7	5.1	5.6	5.8	5.8	5.9
9-8	2.5	3.0	3.2	3.3	3.4
sfc-9	0.7	1.0	1.1	1.1	1.1

6. $g\bar{z} + c_p\bar{T}$ (cal. g.$^{-1}$)

August 25					
Pressure (100's mb.)	Radius (n.mi.) 20	40	60	80	100
2-1.5	83.4	83.2	83.2	83.1	83.1
3-2	82.7	82.5	82.4	82.3	82.3
4-3	80.1	79.9	79.8	79.8	79.8
5-4	78.9	78.7	78.6	78.5	78.5
6-5	77.2	77.0	76.9	76.9	77.0
7-6	75.6	75.5	75.5	75.5	75.5
8-7	74.1	74.0	74.1	74.1	74.1
9-8	72.8	72.7	72.7	72.8	72.8
10-9	71.6	71.6	71.6	71.6	71.6

August 27					
Pressure (100's mb.)	Radius (n.mi.) 15	20	40	60	80
1.5-1	85.1	84.9	84.6	84.5	84.4
2-1.5	83.7	83.7	83.1	82.8	82.5
3-2	82.8	82.7	82.1	82.0	81.7
4-3	81.2	81.2	80.7	80.4	80.2
5-4	79.4	79.5	79.1	78.8	78.6
6-5	77.6	77.9	77.5	77.2	77.0
7-6	75.9	76.2	75.9	75.7	75.6
8-7	74.2	74.6	74.5	74.3	74.1
9-8	72.8	73.2	73.1	73.0	72.9
sfc-9	72.0	72.2	72.2	72.2	72.1

7. $L\bar{q}$ (cal.g.$^{-1}$)

August 25						August 27					
Pressure	Radius (n.mi.)					Pressure	Radius (n.mi.)				
(100's mb.)	20	40	60	80	100	(100's mb.)	15	20	40	60	80
2-1.5	-	-	-	-	-	1.5-1	-	-	-	-	-
3-2	0.2	0.1	0.1	-	-	2-1.5	-	-	-	-	-
4-3	0.9	0.7	0.5	0.4	0.1	3-2	0.7	0.6	0.5	0.3	0.3
5-4	1.8	1.7	1.4	1.2	1.0	4-3	1.9	1.7	1.4	1.2	1.1
6-5	3.5	3.1	3.0	2.7	2.5	5-4	3.5	3.1	2.5	2.4	2.2
7-6	4.9	4.6	4.4	4.3	4.1	6-5	5.2	4.7	4.1	3.7	3.5
8-7	6.6	6.1	6.0	6.0	5.9	7-6	6.9	6.2	5.7	5.1	4.8
9-8	8.2	7.7	7.6	7.5	7.4	8-7	8.4	7.7	5.7	5.1	4.8
10-9	10.6	10.2	9.9	9.7	9.6	9-8	10.0	9.2	8.7	8.1	7.8
						sfc-9	11.8	11.0	10.5	10.3	10.1

8. $\bar{Q} = g\bar{Z} + c_p\bar{T} + L\bar{q}$ (cal. $g.^{-1}$, base 70)

August 25					
Pressure (100's mb.)	Radius (n.mi.) 20	40	60	80	100
2-1.5	13.4	13.2	13.2	13.1	13.1
3-2	12.9	12.6	12.5	12.3	12.3
4-3	11.0	10.6	10.3	10.2	9.9
5-4	10.7	10.4	10.0	9.7	9.5
6-5	10.7	10.1	9.9	9.6	9.5
7-6	10.5	10.1	9.9	9.8	9.6
8-7	10.7	10.1	10.1	10.1	10.0
9-8	11.0	10.4	10.3	10.3	10.2
10-9	12.2	11.8	11.5	11.3	11.2

August 27					
Pressure (100's mb.)	Radius (n.mi.) 15	20	40	60	80
1.5-1	15.1	14.9	14.6	14.5	14.4
2-1.5	13.7	13.7	13.1	12.8	12.5
3-2	13.5	13.3	12.6	12.3	12.0
4-3	13.1	12.9	12.1	11.6	11.3
5-4	12.9	12.6	11.6	11.2	10.8
6-5	12.8	12.6	11.6	10.8	10.4
7-6	12.8	12.4	11.6	10.8	10.4
8-7	12.6	12.3	11.7	10.9	10.3
9-8	12.8	12.4	11.8	11.1	10.7
sfc-9	13.8	13.2	12.7	12.5	12.2